NASA/TM—2010-216100

Spreadsheet Calculations for Jets in Crossflow: Opposed Rows of Inline and Staggered Holes and Single and Opposed Rows With Alternating Hole Sizes

James D. Holdeman
Glenn Research Center, Cleveland, Ohio

James R. Clisset
University of Florida, Gainesville, Florida

Jeffrey P. Moder
Glenn Research Center, Cleveland, Ohio

July 2010

NASA STI Program . . . in Profile

Since its founding, NASA has been dedicated to the advancement of aeronautics and space science. The NASA Scientific and Technical Information (STI) program plays a key part in helping NASA maintain this important role.

The NASA STI Program operates under the auspices of the Agency Chief Information Officer. It collects, organizes, provides for archiving, and disseminates NASA's STI. The NASA STI program provides access to the NASA Aeronautics and Space Database and its public interface, the NASA Technical Reports Server, thus providing one of the largest collections of aeronautical and space science STI in the world. Results are published in both non-NASA channels and by NASA in the NASA STI Report Series, which includes the following report types:

- TECHNICAL PUBLICATION. Reports of completed research or a major significant phase of research that present the results of NASA programs and include extensive data or theoretical analysis. Includes compilations of significant scientific and technical data and information deemed to be of continuing reference value. NASA counterpart of peer-reviewed formal professional papers but has less stringent limitations on manuscript length and extent of graphic presentations.

- TECHNICAL MEMORANDUM. Scientific and technical findings that are preliminary or of specialized interest, e.g., quick release reports, working papers, and bibliographies that contain minimal annotation. Does not contain extensive analysis.

- CONTRACTOR REPORT. Scientific and technical findings by NASA-sponsored contractors and grantees.

- CONFERENCE PUBLICATION. Collected papers from scientific and technical conferences, symposia, seminars, or other meetings sponsored or cosponsored by NASA.

- SPECIAL PUBLICATION. Scientific, technical, or historical information from NASA programs, projects, and missions, often concerned with subjects having substantial public interest.

- TECHNICAL TRANSLATION. English-language translations of foreign scientific and technical material pertinent to NASA's mission.

Specialized services also include creating custom thesauri, building customized databases, organizing and publishing research results.

For more information about the NASA STI program, see the following:

- Access the NASA STI program home page at *http://www.sti.nasa.gov*

- E-mail your question via the Internet to *help@sti.nasa.gov*

- Fax your question to the NASA STI Help Desk at 443–757–5803

- Telephone the NASA STI Help Desk at 443–757–5802

- Write to:
  NASA Center for AeroSpace Information (CASI)
  7115 Standard Drive
  Hanover, MD 21076–1320

NASA/TM—2010-216100

Spreadsheet Calculations for Jets in Crossflow: Opposed Rows of Inline and Staggered Holes and Single and Opposed Rows With Alternating Hole Sizes

James D. Holdeman
Glenn Research Center, Cleveland, Ohio

James R. Clisset
University of Florida, Gainesville, Florida

Jeffrey P. Moder
Glenn Research Center, Cleveland, Ohio

July 2010

Acknowledgments

Level of Review: This material has been technically reviewed by technical management.

Available from

NASA Center for Aerospace Information
7115 Standard Drive
Hanover, MD 21076–1320

National Technical Information Service
5301 Shawnee Road
Alexandria, VA 22312

Available electronically at http://gltrs.grc.nasa.gov

Spreadsheet Calculations for Jets in Crossflow: Opposed Rows of Inline and Staggered Holes and Single and Opposed Rows With Alternating Hole Sizes

James D. Holdeman
National Aeronautics and Space Administration
Glenn Research Center
Cleveland, Ohio 44135

James R. Clisset
University of Florida
Gainesville, Florida 32611

Jeffrey P. Moder
National Aeronautics and Space Administration
Glenn Research Center
Cleveland, Ohio 44135

Abstract

The primary purpose of this jet-in-crossflow study was to calculate expected results for two configurations for which limited or no experimental results have been published, namely:
(1) cases of opposed rows of closely-spaced jets from inline and staggered round holes and
(2) rows of jets from alternating large and small round holes. Simulations of these configurations were performed using a Microsoft Excel (Microsoft Corporation) spreadsheet implementation of a NASA-developed empirical model which had been shown in previous publications to give excellent representations of mean experimental scalar results, suggesting that the NASA empirical model for the scalar field could confidently be used to investigate these configurations. The supplemental Excel spreadsheet is posted with the current report on the NASA Glenn Technical Reports Server (http://gltrs.grc.nasa.gov) and can be accessed from the Supplementary Notes section as TM-2010-216100-SUPPL1.xls. Calculations for cases of opposed rows of jets with the orifices on one side shifted show that staggering can improve the mixing, particularly for cases where jets would overpenetrate slightly if the orifices were in an aligned configuration. The jets from the larger holes dominate the mixture fraction for configurations with a row of large holes opposite a row of smaller ones although the jet penetration was about the same. For single and opposed rows with mixed hole sizes, jets from the larger holes penetrated farther. For all cases investigated, the dimensionless variance of the mixture fraction decreased significantly with increasing downstream distance. However, at a given downstream distance, the variation between cases was smaller.

Introduction

Jets in crossflow (JIC) have been extensively investigated in the literature. The studies of multiple jets that are summarized in Reference 1 were motivated by mixing of dilution jets in conventional gas turbine combustors; and the studies summarized in References 2 and 3 focused on optimizing the mixing section in the Rich burn/Quick mix/Lean burn (RQL) combustor

scheme. Many of the studies summarized in Reference 4 were motivated by aerodynamics associated with vertical/short takeoff and landing aircraft. The summary in Reference 5 focused on calculation methods that have been used for JIC flow fields. References to many of the JIC studies that were published prior to References 1 to 5 are listed in their citations. Because these lists are extensive, older reports and papers are not cited in this publication unless specific results are mentioned. Secondary References are listed parenthetically if the primary Reference is the same as, similar to, or derived from, the secondary Reference.

It was shown in References 1 to 3 that trends of a conserved scalar in JIC flowfields were independent of the duct shape and were similar whether conserved scalar results came from experimental or analytical studies. That is, trends from conserved scalar results could be from probe measurements, nonintrusive species measurements, empirical model calculations, or CFD calculations for nonreacting or reacting flows in a rectangular, annular, or cylindrical duct.

Most JIC research prior to 1970 focused on the trajectory, centerline decay, and the shape of unconfined single jets. The (post 1970) studies in References 6 to 25 were motivated by mixing in the dilution zone of large annular gas turbine combustors, and were based on simplified combustor mixer geometries in a rectangular duct. From the data in Reference 8 a NASA JIC empirical model was reported in Reference 12, published in the journal paper in Reference 13, and used in Reference 15 to illustrate "basic" features of the scalar field downstream of a row of jets mixing with a confined crossflow.

The original NASA JIC empirical model that was published in Reference 13 was subsequently extended to include variations typically found in gas turbine combustors; e.g., noncircular orifices, double and/or opposed rows of jets, with or without flow area convergence and/or a nonuniform mainstream scalar distribution. The experimental and modeling results from the work to include these variations are reported in References 14 and 17 to 19. The NASA JIC empirical model that resulted was used in Reference 20 to demonstrate flow and geometric effects in a rectangular duct. CFD calculations for many of the cases in Reference 14 are given in Reference 21. Journal publications using data from References 14 and 17 to 19 are given in References 1, 16, 22, and 23.

The BASIC programs for the NASA JIC empirical model used in References 15 and 20 were later converted to an Excel (Microsoft Corporation) spreadsheet and reported in Reference 24. Discussions of spreadsheet specifics, cases of jet mixing in a confined crossflow, a slideshow, and a listing of the correlation equations in the NASA JIC empirical model were published in References 24 and 25. Suggested design procedures for cylindrical and rectangular ducts are given in References 2 and 3. Both NASA and Cranfield design methods are discussed in Reference 26.

The primary purpose of this JIC study was to calculate expected results for two configurations for which limited or no experimental results have been published: (1) cases of opposed rows of closely-spaced jets from inline and staggered round holes and (2) rows of jets from alternating large and small round holes. Simulations of these configurations were performed using NASA JIC spreadsheet (described in References 24 and 25) which had been shown in previous publications to give excellent representations of mean experimental scalar results, suggesting that the NASA empirical model for the scalar field could confidently be used to investigate these configurations. The contour plots generated directly in the version of the spreadsheet used herein have considerably less resolution than those presented in Figures 4 to 14 in Reference 25 that were generated with a graphics post processor using data exported from the

spreadsheet. The NASA JIC spreadsheet also generates profile plots, as shown in Figures 4 to 26 in Reference 24 and Figures 15 to 24 and the slideshow in Reference 25.

The first configurations analyzed consist of opposed rows of both inline and staggered arrangements. Results for inline configurations were reported in References 1, 24, 25, and 27. Previously unpublished data for opposed rows of closely-spaced staggered jets from the United Technologies Research Center were used (with permission) in Reference 28. The data used therein were all on a plane of symmetry and were measurements of velocity magnitude rather than a conserved scalar. Some other unpublished measurements were made off a plane of symmetry (private communication with D.S. Liscinsky).

The second configurations analyzed were rows of jets with alternating hole sizes. There are no data in the open literature for opposed rows of jets from alternating hole sizes, but there were experimental results for one-side injection from mixed size holes reported in Reference 8, and data were published in Reference 27 for opposed rows of aligned jets. Adjacent jets in Reference 27 were always the same size, but cases were investigated with different size holes on opposite sides.

Nomenclature

A_J/A_M jet-to-mainstream area ratio $= (\pi/4)/((S/d)(H/d)) = (\pi/4)/((S/H)(H/d)^2)$

C jet penetration coefficient $= (S/H)(\sqrt{(J)})$; same as Equation (5)

C_d orifice discharge coefficient $=$ (effective area)/(physical area)

d actual physical diameter of a round hole

d_j effective diameter $= (d)(\sqrt{(C_d)})$

DR jet-to-mainstream density ratio, ρ_J/ρ_M

H duct height at center of row of holes (called H_0 in several previous publications)

H/d ratio of duct height to orifice diameter

H_{eq} effective duct height ($= H$ except in the symmetry model for opposed rows of inline jets)

J jet-to-mainstream momentum-flux ratio, $(\rho_J V_J^2)/(\rho_M U_M^2)$

m_J jet mass flow

m_M mainstream mass flow

m_T total mass flow, $m_J + m_M$

m_J/m_M jet-to-mainstream mass-flow ratio $= (\rho_J/\rho_M)(V_J/U_M)(C_d)(A_J/A_M)) = (m_J/m_T)/(1 - m_J/m_T)$

m_J/m_T jet-to-total mass-flow ratio

S   lateral spacing between equivalent locations of adjacent orifices, e.g., between orifice centerplanes

S/d ratio of lateral orifice spacing to orifice diameter $= (S/H)(H/d)$

S/H ratio of lateral orifice spacing to duct height

S_X/H ratio of axial orifice spacing to duct height

T local scalar variable

T_J scalar variable at jet exit

T_M scalar variable in unmixed mainstream flow

U axial velocity

U_M unmixed mainstream velocity

U_s unmixedness = $\theta_{var}/(\theta_{ave}(1 - \theta_{ave}))$; same as Eq. (4)

V_J jet exit velocity

$W_{1/2}^-$ jet half-value width on injection side of vertical distribution; i.e., for $y/H < y_c/H$ in Figure 2 (note that $y = 0$ is at the top wall)

$W_{1/2}^+$ jet half-value width on opposite side of vertical distribution; i.e., for $y/H > y_c/H$ in Figure 2 (note that $y = 0$ is at the top wall)

x downstream coordinate; $x = 0$ at center of the first row of orifices

y cross-stream coordinate; $y = 0$ at wall

y_c scalar trajectory, location of maximum scalar difference ratio, θ_c

z lateral coordinate; $z = 0$ at centerplanes

θ dimensionless scalar, $(T_M - T)/(T_M - T_J)$; same as Equation (2)

θ_{ave} fully-mixed scalar difference ratio = θ_{EB}

θ_c maximum scalar difference ratio, defines location of scalar trajectory, y_c/H

θ_{EB} equilibrium θ (called TB in Reference 15) approximately m_J/m_T

θ_{min}^- minimum scalar difference ratio on injection side of vertical distribution; (i.e., for $y/H < y_c/H$ in Figure 2)

θ_{min}^+ minimum scalar difference ratio on opposite side of vertical distribution; (i.e., for $y/H > y_c/H$ in Figure 2)

θ_{var} variance of scalar difference ratio

Flow Field Model

Figure 1 is a schematic of the basic flow field for jets in a confined crossflow. The jets are shown entering the mainstream flow through orifices in the top duct wall. The primary independent geometric variables are the lateral spacing between similar locations of adjacent orifices S, the duct height H, and the orifice diameter d. S/H and H/d were chosen as independent dimensionless variables. The product of them, the ratio of the orifice spacing to orifice diameter S/d is a frequently cited dimensionless variable. Note that for round holes S/d cannot be less than 1.

Downstream distances are specified in intervals of x/H because the objective in combustor design is usually to identify orifice configurations to optimize the mixing within a given length and the downstream locations of interest are usually independent of the orifice diameter. The ratio of the downstream distance to the orifice diameter $x/d = (x/H)(H/d)$ is a common dimensionless parameter, particularly in unconfined flows.

The empirical model for the conserved scalar field downstream of jets mixing with a confined crossflow is based on the observation that nondimensional vertical scalar distributions in the flow field can usually be expressed in the following form

$$\frac{\theta - \theta_{min}^{\pm}}{\theta_c - \theta_{min}^{\pm}} = \exp\frac{(-\ln 2)(y/H - y_c/H)}{(W_{1/2}^{\pm}/H)} \tag{1}$$

where

$$\theta = (T_M - T)/(T_M - T_J) \tag{2}$$

θ_c, θ_{min}^+, θ_{min}^-, $W_{1/2}^+\big/H$, $W_{1/2}^-\big/H$, and y_c/H in Eq. (1) are scaling parameters for θ profiles in a vertical x-y plane as shown in Figure 2. Note that $x = 0$ is at the center of the orifice and $y = 0$ is at the top in Figures 1 and 2, and that the jet trajectory y_c/H is defined as the location of the maximum scalar difference in the profile in the centerplane (the x-y plane though the center of an orifice). Unmixed jet fluid is $\theta = 1$ and unmixed mainstream fluid is $\theta = 0$. A physically realistic θ should be neither <0 nor >1. Although θ was formulated from temperature data in an incompressible flow in References 8, 14, 17, and 18, θ applies to any conserved scalar. For example, species concentration was often used in the isothermal experimental studies summarized in References 2 and 3 and a carbon balance was used in the experiments results for reacting flows reported in References 2 and 29 to 31.

Equation (1) was first applied to confined JIC data in Reference 11. It gives $\theta = (\theta_c + \theta_{min}^{\pm})/2$ at the half-value width $W_{1/2}^{\pm}\big/H$ on the opposite or injection side of the trajectory as appropriate, but does not guarantee that $\theta = \theta_{min}^-$ at $y = 0$ or $\theta = \theta_{min}^+$ at H. Usually $\theta_{min}^+ \neq \theta_{min}^-$ and $W_{1/2}^+\big/H \neq W_{1/2}^-\big/H$. Off-centerplane values of θ_c and y_c are dependent on z, and it is assumed in the empirical model that off-centerplane values of $\theta_{min}^{\pm}/\theta_c$ and $W_{1/2}^{\pm}\big/H$ are equal to their values in the centerplane. Calculations at y/H should not be accepted if $y/H<0$ or $y/H>1$ and should be scrutinized carefully if $y/H<y_c/H$ and $(y_c/H - W_{1/2}^-\big/H) < 0$ or if $y/H > y_c/H$ and $(y_c/H + W_{1/2}^+\big/H) > 1$.

An equation similar to Equation (1) was applied to data for a single, unconfined JIC ($\theta_{min}^{\pm} = 0$) in References 6 and 7.

Correlation equations were developed for each of the scaling parameters and are given in Reference 24. For all calculations, the dimensionless flow and geometric variables that must be specified are the jet-to-mainstream density ratio DR, jet-to-mainstream momentum-flux ratio J, jet discharge coefficient C_d, orifice-spacing-to-duct-height ratio S/H, duct-height-to-orifice-diameter ratio H/d, and the dimensionless downstream distance x/H. If there are multiple rows of jets, the axial distance between their centers S_X/H must also be specified.

The correlation equations used in the spreadsheet are the same as those included in Reference 1, but the equations published there are written in terms of H_{eq} and H_0 rather than H. For all the cases considered here $H_0 = H_{eq} = H$, since $H_0 = H$ in a nonconverging duct and H_{eq} is only $\neq H$ if the symmetry model is used for opposed rows of jets with their centerlines inline. Most of the cases for this application are in the near field of the JIC, so, although the trajectory becomes asymptotic in the axial direction, characterization of the flow depends on both downstream distance and JIC configuration.

Three-dimensional oblique plots (herein called profile plots) and low resolution contour plots are the native displays in the spreadsheet. The dependent variable θ is shown on the horizontal axis in the profile plots and θ is the plotted variable in the contour plots. The vertical and oblique axes in the profile plots are the y and z directions, which are respectively in the direction of the jet injection and along the orifice row in an axial plane. These are the axes of ordinates and abscissas in the contour plots. There are 21 profiles in the z-span shown in the figures, but less than half of the jet profiles are actually calculated directly. The others are generated by assuming cyclic boundary conditions at the jet centerplanes or midplanes as appropriate. (The x-y plane through the orifice center is called the centerplane, and that halfway between orifices in each row is called the midplane.)

The downstream distance x/H and orifice spacing S/H must be input in the top front row in the spreadsheet. S/H and x/H for other rows are dependent on, but may not be identical to, the values input there. The specifics and operation of the spreadsheet, the correlations in the NASA empirical model, the "closest" experimental data, and listings of the original BASIC programs are given in Reference 24.

Because of the positive results using the superposition model for inline jets shown in Reference 25, the superposition model was used for all opposed row conditions. Profiles for multiple rows were obtained by combining independent calculations of the flow distributions according to the following equation:

$$\theta = \frac{\left[\theta_1 + \theta_2 - 2(\theta_1)(\theta_2)\right]}{\left[1 - (\theta_1)(\theta_2)\right]}$$

(3)

For opposed rows of jets with centerlines inline, θ_1 is the distribution for the top and θ_2 is the distribution for the bottom. If there are more than 2θ's, Equation (3) is used up to three more times to get a function of, at most, five θ's (a JIC spreadsheet maximum).

Although superposition usually gives a good approximation to the experimental data, it should be realized that it is an approximation, since there may be an interaction between opposite and/or adjacent jets that is not accounted for in superimposing independently calculated distributions.

The older symmetry model, described in e.g., References 1, 15, 20, and 23 to 25, is still the default method in the spreadsheet for opposed rows of jets with their centerlines aligned. Specifying anything other than slanted slots in the same row with all orifices aligned uses symmetry. To invoke the superposition model, one must not have the same configurations on both top and bottom in any row. The "solution" to get superposition for two opposed rows of jets with their centerlines aligned is to use row 1 top and row 2 bottom (or row 2 top and row 1 bottom) and to specify $S_X/H = 0$.

The NASA JIC empirical model assumes the flows of interest will be confined and cannot be used for unconfined jet flows because the relations used for orifice size and spacing do not extrapolate properly as jet spacing and/or the distance to the opposite wall becomes large. Although it may work, the spreadsheet should not be used upstream of the trailing edge of the orifices.

Per Reference 27, the unmixedness U_s is defined as

$$U_s = \frac{\theta_{\text{var}}}{\theta_{ave}(1 - \theta_{ave})}$$

(4)

where θ_{var} is the mean squared deviation between θ_{ave} and all θ values in the span shown at each axial x location for which calculations are performed (in this case, 2020 θ – values = 20 profiles × 101 spanwise points, where the 21st profile is not included in the average because it is the beginning of the next cycle). θ_{ave} is the fully-mixed mean value (usually = m_J/m_T) and is not a function of the axial location x.

Analysis of the experimental data in References 8 and 14 suggested a coupling between the orifice spacing and the momentum-flux ratio, and led to the conclusion that similar penetration occurs independent of orifice size if the square root of the momentum-flux ratio J and orifice spacing S/H are inversely proportional. This relationship can be stated as

$$C = (S/H)(\sqrt{J}) \tag{5}$$

Equation (5) for the jet penetration coefficient C is not assumed in the correlations, so the empirical model results shown in References 1, 13, 15, 20, and 22 to 25 and this report provide verification for it.

The coefficient C can be useful in characterizing the jet penetration. For one sided injection, optimum penetration was found to occur when C was approximately 2.5. Obvious under-penetration was observed when C was half the optimum value, and obvious over-penetration was observed when C was double the optimum value. For opposed rows of inline jets, the corresponding C values are half of those above; for opposed rows of staggered jets, the corresponding C values are double the single-side ones. As can be seen from Equation (5), and inferred from perusing the figures in References 24 and 25, there is usually a trade-off between momentum-flux ratio J and orifice spacing S/H. Note that C characterizes penetration rather that mixing, but it usually follows that an optimum C gives the best mixing at a given J. Mixing parameters, such as the standard deviation of the mixture fraction, and the "unmixedness" U_s, should be consistent with the θ distribution. Having shown that it is, mixing parameter values can be compared, but comparing mixing parameters alone can be misleading as a nonoptimum configuration at one J can have, for example, a lower U_s than for an optimum configuration at a lower J.

Review of Significant Flow and Geometry Effects

Figures 3 to 7 are similar to Figures 9 to 14 in References 24 and 25, except that both the contour and profile plots here are from the spreadsheet posted with this report, whereas the contour plots in Figures 4 to 14 in Reference 25 were done with a graphics post-processor from spreadsheet data. Although the same trends could be shown at different axial locations, results in Figures 3 to 7 are shown at a downstream distance equal to one half of the duct height ($x/H = 0.5$). These cases were initially run to check results from the current spreadsheet but are included in this report as they provide background material for the new results.

Variation of θ Distributions With Momentum-Flux Ratio (J)

The momentum-flux ratio J is the most significant flow variable. Figure 3 shows the increase in jet penetration that occurs with increasing momentum-flux ratio ($6.6 \leq J \leq 105.6$); here $S/H = 0.5$ and $H/d = 5.66$. Note that the jets are under-penetrating in Figure 3(a) ($C = 1.28$), optimum in Figure 3(b) ($C = 2.57$), and over-penetrating in Figure 3(c) ($C = 5.14$). Since the orifice size and spacing are constant the jet-to-mainstream mass-flow ratio MR increases with increasing momentum-flux ratio J.

Variation of θ Distributions With Density Ratio (DR) for a Constant Momentum-Flux Ratio (J)

Analyses of the experimental data in References 8 and 14 showed that the effect of varying the density ratio DR was minor when J was constant. This effect can be seen in Figure 4. In the figure, the density ratio varies from 0.5 (less dense jets) to 1 (equal density) to 2 (more dense jets). In Figure 4, $J = 26.4$, $S/H = 0.5$ ($C = 2.57$), with $H/d = 5.66$. Note that the magnitude of θ increases slightly as the density ratio increases because the jet-to-mainstream mass-flow ratio increases as the density ratio increases. Other than this, there is not much difference between hot-jets-in-a-cold-mainstream and cold-jets-in-a-hot-mainstream at a constant momentum-flux ratio.

Variation of θ Distributions With Orifice Spacing (*S/H* and *S/D*) at a Constant Orifice Size (*H/D*)

Figure 5 shows the effect of increasing the lateral spacing between orifices from $S/H = 0.25$ to 1.0 ($2 \leq S/d \leq 8$) with $J = 26.4$ and $H/d = 8$. The jet penetration increases as S/H increases ($1.28 \leq C \leq 5.14$). Note that the lateral variation of the distribution also increases as orifice spacing increases. Both this and the increased jet penetration probably occur because there is less interaction between adjacent jets when they are farther apart. The jet-to-mainstream mass-flow ratio decreases as the spacing increases, since the orifice size is constant.

Variation of θ Distributions With Orifice Size (*H/D*) at a Constant Orifice Spacing (*S/H*)

The jet penetration in Figure 6 remains very similar when the orifice diameter *d* increases (*H/d* decreases) at a constant *S/H*. (Note that *S/H* is constant, but *S/d* is proportional to *H/d*.) The orifice diameter doubles as *H/d* is varied from 8 to 4, resulting in a four-fold increase in the jet-to-mainstream mass-flow ratio *MR*. The result is that the distributions shift to higher θ values as *MR* increases, but the jet penetration and shape of the distributions remains similar. The obvious conclusion from Figure 6 is that varying the orifice size has a secondary effect on jet penetration. Orifice size can be chosen to satisfy other considerations (e.g., the mass-flow ratio) provided *S/H* is constant. Note that when *S/H* and *x/H* are constant both *S/d* and *x/d* decrease as *H/d* decreases.

Variation of θ Distributions With Coupled Orifice Spacing (S/H) and Momentum-Flux Ratio (*J*)

The plots in Figure 7 show the inverse relationship between the orifice spacing *S/H* and the momentum-flux ratio *J* when they are related according to Equation (5); e.g., for $J = 6.6$, $S/H = 1$; for $J = 26.4$, $S/H = 0.5$; and for $J = 105.6$, $S/H = 0.25$. The conditions in Figure 7 represent nearly optimum mixing conditions for a single row of jets ($C = 2.57$), although similar trends could be shown for over- and under-penetrating jets. In Figure 7 the mass-flow ratio *MR* is constant, because the orifice size was decreased as the momentum-flux ratio *J* was increased and the orifice spacing *S/H* was decreased. Clearly, similar penetration is obtained over a range of momentum-flux ratios if *J* and *S/H* are coupled, but note also that the flow is vertically and laterally less uniform for smaller momentum-flux ratios. This result was shown in Reference 1 using experimental data.

Results and Discussion

Figures 8 to 20 show results for the primary configurations investigated here: (1) opposed rows of inline and staggered jets and (2) rows of jets from alternating large and small holes. Results for the conditions investigated computationally are shown in the contour and profile plots in Figures 8 to 20 and the conditions for the calculations are given in Table 1 and also identified in the titles of the figures. The downstream location and the unmixedness U_s are given in the subtitle for each part of each figure. Recall that the $x = 0$ location is at the center of the holes, and note that the trailing edge of round holes is at $x/H = (0.5)/(H/d)$. Because the "effective" duct height for opposed rows is often approximately half of the actual duct height, downstream locations of $x/H = 0.125$, 0.25, and 0.5 were chosen for opposed rows of jets and $x/H = 0.25$, 0.5, and 1.0 were chosen for most of the single-side injection cases.

Figures 8 to 15 show opposed rows of inline and staggered jets for cases that either are optimum configurations for one side injection or are optimum for opposed rows of inline jets. Figures 16 to 20 show a single row and opposed rows of jets from alternating large and small holes. There is a considerable decrease in U_s with downstream distance for each case shown in

Figures 8 to 20, however, there is also a smaller difference in U_s between cases at a given downstream location.

Opposed Rows of Inline and Staggered Jets

Inline Jets

The cases in Figures 8 and 9 are similar to the results for single and opposed rows of inline jets in References 1, 15, 20, 24, 25, and 27. The experimental data in Reference 27 show that jets from opposite walls penetrate similarly in inline configurations for the same momentum-flux ratio J even if the orifice sizes on opposite sides are different.

Figure 8 is a nearly optimum configuration for opposed rows of inline jets. Note that the jets penetrate to approximately $H/4$ and that $C = 1.28$ for the configuration shown. Figure 9 has double the S/H, but the diameter of the holes is increased to give the same total area ($A_J/A_M = 0.098$). For this case, the jets penetrate to approximately $H/2$ and $C = 2.57$. As this is a nearly optimum configuration for one side injection, the overpenetration shown in Figure 9 for opposed rows of inline jets is expected. Figure 10 has the same total area, momentum-flux ratio, and orifice spacing as Figure 9 but with smaller holes ($H/d = 8$) on top and larger ones ($H/d = 4.62$) on the bottom ($C = 2.57$ on both sides). The cases in Figures 9 and 10 confirm the earlier results that hole size has a minimal effect on penetration for jets at the same spacing S/H and momentum-flux ratio J. As the smaller holes get smaller (and eventually disappear), and the larger ones get larger, they approach the limit of optimum single-side injection, which is shown in Figure 11.

The U_s values for Figures 9 and 10 are similar, but the unmixedness for the case in Figure 10 with different hole sizes on opposite walls is a little bit higher than the case in Figure 9 where the holes are all the same size. However, the U_s values in Figure 11 for single-side injection with $H/d = 4$ is higher still. The lowest U_s is for the optimum configuration for opposed rows as shown in Figure 8.

Staggered Jets

A configuration for optimum penetration of staggered jets is shown in Figure 12 for $A_J/A_M = 0.098$. A staggered optimum is obtained when every other hole of an optimum configuration for one-side injection is relocated to the opposite side. Thus, for an optimum staggered configuration, the spacing of adjacent jets is doubled from that for a single side optimum. The unmixedness U_s is slightly less for the optimum staggered configuration than for the single side optimum, but U_s for an optimum staggered configuration (Fig. 12) is significantly larger than for an optimum inline configuration (Fig. 8) probably because there are four times as many holes in an optimum inline configuration.

Because C for an optimum staggered configuration is quadruple the optimum for opposed rows of inline jets, the diameter of round holes for an optimum staggered configuration is twice that for jets in an opposed inline optimum for the same area ratio. If C is less than the optimum for a staggered configuration, the penetration of staggered jets will be reduced. For example, note that the orifice spacing for the case in Figure 13 ($S/H = 0.5$) is half of that for the optimum staggered case in Figure 12 ($S/H = 1.0$).

The cases in Figures 13 and 14 are similar respectively to those in Figures 9 and 10 except that the lower row of holes in Figures 13 and 14 are shifted by $S/2$. The staggered jet cases shown in Figures 13 and 14 overpenetrate if opposed jets are inline. In Figure 13 all the holes are

the same size ($H/d = 5.66$), whereas the case in Figure 14 has smaller holes ($H/d = 8$) on top and larger ones ($H/d = 4.62$) on the bottom. The cyclical nature of the results shown in Figure 13 is confirmed by unpublished measurements from UTRC (private communication) for the staggered jet case described in Reference 28. As in Figures 9 and 10 which are inline configurations, the unmixedness U_s in Figure 13 where the holes are all the same size is a little bit less than that in Figure 14 with different holes sizes on opposite sides.

Also of interest is a comparison of inline and staggered configurations where the staggered one has a row shifted such that the centerplane of the jets from one side is opposite from the midplane of jets from the opposite side. θ distributions in Figures 9 and 13 and 10 and 14 suggest that an opposed row of staggered jets in a nearly optimum configuration for one-side injection mix better than an opposed row of inline ones at the same spacing and momentum-flux ratio, however the U_s for the staggered cases are only slightly less than for the inline cases. For an optimal configuration for opposed rows of inline jets (as in Fig. 8), shifting does not make much difference as shown in Figures 8 and 15.

Rows of Jets From Alternating Large and Small Holes

One-Side Injection From Orifices With Mixed Hole Sizes

The cases shown in Figures 16 to 18 are similar to those in Reference 8. In addition to the alternating size holes in Figure 18, these include the cases of only large holes at the spacing between holes of the same size in the alternating-size configuration (Fig. 16) and uniform size holes at the spacing between adjacent holes in the mixed configuration (Fig. 17). Note that the case shown in Figure 18 is a combination of the cases shown in Figures 16 and 17 so the total area in Figure 18 is $A_J/A_M = 0.098$. Also note that two jets are shown in Figure 17, whereas four of the smaller jets are shown in Figure 18 and that the U_s values in Figures 16 to 18 are comparable to many of those for the opposed row cases, but the downstream distances in Figures 16 to 18 are double those for opposed rows. Faster mixing is typical for opposed rows as there are usually more and smaller holes in configurations with opposed rows of inline jets than in one-side configurations.

The penetration of the jets was shown previously, with both experimental and modeling results (e.g., Refs. 1, 15, 20, 24, and 25), to be largely independent of orifice size, so the jet penetration would be expected to be about the same for adjacent holes if the same spacing was used for both the large and small holes. This is contrary to the experimental results in Reference 8 that shows that jets from the larger holes penetrate farther.

To implement mixed hole sizes in the JIC spreadsheet we used both rows on top with the axial spacing $S_x/H = 0$ and the lateral spacing S/H between large holes for the large holes and the lateral spacing between all holes for the small holes. Although the lateral spacing S/H is input only in row1-top in the spreadsheet, it is divided by two for the smaller holes by specifying four holes for them and two holes for the larger ones. This changes the penetration of adjacent jets significantly although they have the same J.

This is shown in the spreadsheet calculations in Figure 18 for alternating size holes for injection from one side (here the top) for $A_J/A_M = 0.098$. Each row of the mixed hole size configuration in this simulation is half of the total area. However, because there are only half as many large holes and because a larger hole is co-resident with a smaller one in the calculation, the effective area of the large holes is really three times that of the small ones. The jets from the large holes overpenetrate as expected, because the S/H between large holes is too big ($S/H = 1$)

for this momentum-flux ratio ($J = 26.4$), whereas the spacing of the small holes is nearly optimum ($S/H = 0.5$).

Opposed Rows of Jets With Mixed Hole Sizes

The results in Figures 16 to 18 for one-side injection of jets in crossflow agree with the experimental data in Reference 8 so the JIC spreadsheet was used to calculate expected results for opposed rows of jets with mixed hole sizes. For opposed rows of mixed hole sizes, we used both rows on top and bottom with $S_x/H = 0$ and again used the lateral spacing S/H between large holes for the large holes and the lateral spacing between all holes for the small holes.

For opposed rows with holes of mixed sizes, there are two possible configurations—holes of the same size can be opposite each other, or a larger hole can be opposite a smaller one. These are shown in Figures 19 and 20 for a total $A_J/A_M = 0.098$. Although the θ distributions suggest significantly better mixing in the staggered configuration in Figure 20, the U_s values are only slightly lower for the staggered configuration. The limiting cases are (1) all holes are of the same size and (2) only the large holes exist. These are shown in Figures 8 and 9 for opposed rows of inline jets for a nearly optimum opposed row configuration for inline jets (Fig. 8) and an opposed row configuration of larger holes with double the orifice spacing (Fig. 9). Corresponding staggered configurations are shown in Figures 15 and 13, respectively. The mixing for the case in Figure 13 of staggered jets at a spacing that is optimal for one-side injection ($C = 2.57$) appears to be significantly better than that for inline jets as in Figure 9, but for jets in a nearly optimal configuration for opposed rows of inline jets ($C = 1.28$), staggering does not make much difference, as shown in Figures 8 and 15.

The Unmixedness U_s for opposed rows of jets with mixed hole sizes is about the same for both inline (Fig. 19) and staggered (Fig. 20) configurations, but U_s is usually slightly smaller for the staggered case. Also the U_s values for both inline and staggered cases with mixed hole sizes are less than U_s for only large holes with $C = 2.57$ as shown in Figures 9 and 13. However, the U_S for jets in a nearly optimal configuration for opposed rows of inline jets is about the same whether the jets are staggered or inline, as shown in Figures 8 and 15.

Conclusions

A spreadsheet which displays 3–D plots of the distributions of a conserved scalar downstream of jets mixing with a confined crossflow was used to investigate the cases of opposed rows of jets in inline and staggered configurations and single and opposed rows of alternating large and small holes. The spreadsheet used in this report is the same as that posted with NASA/TM—2006-214226 except that contour plots were added to the Excel spreadsheet.

Previous publications showed that the NASA empirical model gave results that were an excellent representation of mean experimental results so that the model could confidently be used to investigate opposed rows of jets in inline and staggered configurations with uniform size and alternating large and small holes. Although closely-spaced staggered jets are usually not an optimum staggered configuration, shifting of one side to make a staggered configuration from one in which opposed jets are aligned can improve the mixing, particularly for cases that would overpenetrate slightly when the orifices are in an aligned configurations. For single and opposed rows of mixed size holes, jets from the larger holes penetrated farther and dominated the mixture fraction. For all cases investigated, staggered configurations mixed better than comparable

unshifted inline ones. However, optimum configurations for opposed rows of inline jets mixed significantly faster than optimum one-side or optimum staggered opposed row configurations.

The dimensionless variance of the mixture fraction decreased significantly with increasing downstream distance for all cases. Although the variation between cases at the same downstream distance was smaller, it was consistently lower for staggered configurations. The unmixedness for optimum configurations for opposed rows of inline jets was significantly less than the unmixedness for optimum one-side or optimum staggered opposed row configurations.

References

1. Holdeman, J.D., Mixing of Multiple Jets With a Confined Subsonic Crossflow. *Progress in Energy and Combustion Science*, Vol. 19, pp. 31–70, August 1993 (similar to AIAA Paper 91–2458 and NASA TM–104412, June 1991).
2. Holdeman, James D., Liscinsky, David S., Oechsle, Victor L., Samuelsen, G. Scott, and Smith, Clifford E., Mixing of Multiple Jets With a Confined Subsonic Crossflow: Part I—Cylindrical Ducts. *Journal of Engineering for Gas Turbines and Power*, Vol.119, October 1997 (same as ASME Paper 96–GT–482 and NASA TM–107185, June 1996).
3. Holdeman, J.D., Liscinsky, D.S., and Bain, D.B., Mixing of Multiple Jets With a Confined Crossflow: Part II—Opposed Rows of Orifices in Rectangular Ducts. *Journal of Engineering for Gas Turbines and Power*, Vol.121, July 1999 (same as ASME Paper 97–GT–439 and NASA TM–107461, June 1997).
4. Margason, R.J., Fifty Years of Jet in Cross Flow Research, Presented at Computational and Experimental Assessment of Jets in Cross Flow, AGARD Conference Proceedings 534, April 1993.
5. Demuren, A.O., Modeling Jets in Cross Flow. NASA Contractor Report 194965 (same as ICASE Report No. 94–71), August 1994.
6. Holdeman, James D., Correlation for Temperature Profiles in the Plane of Symmetry Downstream of a Jet Injected Normal to a Crossflow. NASA TN D–6966, September 1972.
7. Kamotani, Y. and Greber, I., Experiments on a Turbulent Jet in a Cross Flow. *AIAA Journal*. Vol.10, No.11, pp. 1425–1429, November 1972 (same as AIAA Paper 72–149, January 1972; derived from NASA CR–72893, June 1971).
8. Walker, R.E. and Kors, D.L., Multiple Jet Study Final Report. NASA CR–121217, June 1973.
9. Holdeman, J.D., Walker, R.E., and Kors, D.L., Mixing of Multiple Dilution Jets With a Hot Primary Airstream for Gas Turbine Combustors. AIAA Paper 73–1249, November 1973 (same as NASA TM X–71426).
10. Walker, R.E., Kors, D.L., and Holdeman, J.D., Mixing of Multiple Jets of Cooling Air With Simulated Combustion Gases. CPIA Publication 243, Proceedings of the 10th JANNAF Combustion Meeting, Vol. I, pp. 377– 396, December 1973.
11. Kamotani, Y. and Greber, I., Experiments on Confined Turbulent Jets in Cross Flow, NASA CR–2392, March 1974.
12. Walker, R.E. and Eberhardt, R.G., Multiple Jet Study Data Correlations, NASA CR–134795, April 1975.
13. Holdeman, J.D. and Walker, R.E., Mixing of a Row of Jets with a Confined Crossflow. *AIAA Journal*, Vol. 15, No. 2, pp. 243–249, February 1977 (similar to AIAA Paper 76–48 and NASA TM X–71821, January 1976).
14. Srinivasan, R., Berenfeld, A., and Mongia, H.C., Dilution Jet Mixing Program Phase I Report. NASA CR–168031 (Garrett 21–4302), November 1982.
15. Holdeman, J.D., Perspectives on the Mixing of a Row of Jets with a Confined Crossflow. AIAA Paper 83–1200 (same as NASA TM–83457), June 1983.

16. Holdeman, J. D., Srinivasan, R., and Berenfeld, A., Experiments in Dilution Jet Mixing. *AIAA Journal,* Vol. 22, No. 10, pp. 1436–1443, October 1984 (same as AIAA Paper 83–1201 and NASA TM–83434, June 1983).

17. Srinivasan, R., Coleman, E., and Johnson, K., Dilution Jet Mixing Program Phase II Report. NASA CR–174624 (Garrett 21–4804), June 1984.

18. Srinivasan, R., Meyers, G., Coleman, E., and White, C., Dilution Jet Mixing Program Phase III Report. NASA CR–174884 (Garrett 21–5418), June 1985.

19. Srinivasan, R. and White, C.D., Dilution Jet Mixing Program Supplementary Report. NASA CR–175043 (Garrett 21–5705), March 1986.

20. Holdeman, J.D., and Srinivasan, R., Perspectives on Dilution Jet Mixing. AIAA Paper 86–1611 (same as NASA TM–87294), June 1986.

21. Srinivasan. R., Reynolds, R., Ball, I., Berry, R., Johnson, K., and Mongia, H., Aerothermal Modelling Program: Phase I Final Report, Volume II. NASA CR–168243 (Garrett 21–4742–2), August 1983.

22. Holdeman, J.D. and Srinivasan, R., Modeling Dilution Jet Flowfields. *Journal of Propulsion and Power*, Vol. 2, No. 1, January–February 1986, pp. 4–9 (similar to AIAA Paper 84–1379 and NASA TM–83708, June 1984).

23. Holdeman, J.D., Srinivasan, R., Meyers, G.D., and White, C.D., Effects of Multiple Rows and Noncircular Orifices on Dilution Jet Mixing. *Journal of Propulsion and Power*, Vol. 3, No. 3, May–June 1987, pp. 219–226 (similar to AIAA Paper 85–1104 and NASA TM–86996, July 1985).

24. Holdeman, J.D., Smith, T.D., Clisset, J.R., and Lear, W.E., A Spreadsheet for the Mixing of a Row of Jets with a Confined Crossflow, NASA/TM—2005-213137, February 2005.

25. Holdeman, J.D., Clisset, J.R., Moder, J.P., and Lear, W.E., On the Mixing of Single and Opposed Rows of Jets With a Confined Crossflow, NASA/TM—2006-214226, October 2006.

26. Lefebvre, Arthur H., *Gas Turbine Combustion, Second Edition,* Taylor and Francis, 1999.

27. Liscinsky, D.S., True, B. and Holdeman, J.D., Effect of Inlet Flow Conditions on Crossflow Jet Mixing. AIAA Paper 96–2881 (same as NASA TM–107258), July 1996.

28. Kobayashi, H., Ham, F., and Wu, X., Application of a local SGS model based on coherent structures to complex geometries. *International Journal of Heat and Fluid Flow*, Vol, 29, pp.640–653, 2008.

29. Leong, M.Y., Samuelsen, G.S., and Holdeman, J.D., Mixing of Jet Air With a Fuel-Rich, Reacting Crossflow, *Journal of Propulsion and Power,* Vol. 15, No. 5, September–October 1999, pp. 617–622 (similar to WSS/CI Paper No. 97S–034 & NASA TM 107430, Apr. 1997, derived from NASA CR–195375, Sept. 1996).

30. Leong, M.Y., Samuelsen G.S., and Holdeman, J.D., Optimization of Jet Mixing into a Rich, Reacting Crossflow, *Journal of Propulsion and Power,* Vol. 16, No. 5, September–October 2000, pp. 729–735 (same as AIAA–98–0156 and NASA/TM—1997-206294, Dec. 1997; derived from NASA CR–195375, Sept. 1996).

31. Holdeman, J.D. and Chang, C.T., Mixing of Multiple Jets With a Confined Subsonic Crossflow: Part III—The Effects of Air Preheat and Number of Orifices on Flow and Emissions in an RQL Mixing Section. NASA/TM—2008-215151, March 2008 (similar to *Journal of Fluids Engineering*, Vol.129, pp.1460–1467, November 2007; derived from NASA/TM—1999-209431, September 1999).

TABLE 1.—CONDITIONS INVESTIGATED

Case/figure no.	S/H	S/d	H/d	A_J/A_M	J	C^a
opposed row inline		optimum				
8 top	0.25	2	8	0.0491	26.4	1.28
bottom	0.25	2	8	0.0491	26.4	1.28
opposed row inline						
9 top	0.5	2.83	5.66	0.0491	26.4	2.57
bottom	0.5	2.83	5.66	0.0491	26.4	2.57
10 top	0.5	4	8	0.0245	26.4	2.57
bottom	0.5	2.31	4.62	0.0737	26.4	2.57
single side		optimum				
11	0.5	2	4	0.0982	26.4	2.57
opposed row staggered		optimum				
12 top	1	4	4	0.0491	26.4	5.14
bottom	1	4	4	0.0491	26.4	5.14
opposed row staggered						
13 top	0.5	2.83	5.66	0.0491	26.4	2.57
bottom	0.5	2.83	5.66	0.0491	26.4	2.57
14 top	0.5	4	8	0.0245	26.4	2.57
bottom	0.5	2.31	4.62	0.0737	26.4	2.57
15 top	0.25	2	8	0.0491	26.4	1.28
bottom	0.25	2	8	0.0491	26.4	1.28
single side limits						
16	1	4	4	0.0491	26.4	5.14
17	0.5	2,83	5.66	0.0491	26.4	2.57
single side mixed size						
18	1	4	4	0.0491	26.4	5.14
+	0.5	2,83	5.66	0.0491	26.4	2.57
opposed row mixed size		inline				
19 top	0.5	4	8	0.0245	26.4	2.57
+	0.25	2.83	11.31	0.0245	26.4	1.28
bottom	0.5	4	8	0.0245	26.4	2.57
+	0.25	2.83	11.31	0.0245	26.4	1.28
opposed row mixed size		staggered				
20 top	0.5	4	8	0.0245	26.4	2.57
+	0.25	2.83	11.31	0.0245	26.4	1.28
bottom	0.5	4	8	0.0245	26.4	2.57
+	0.25	2.83	11.31	0.0245	26.4	1.28

$^aC = (S/H)(\surd(J))$
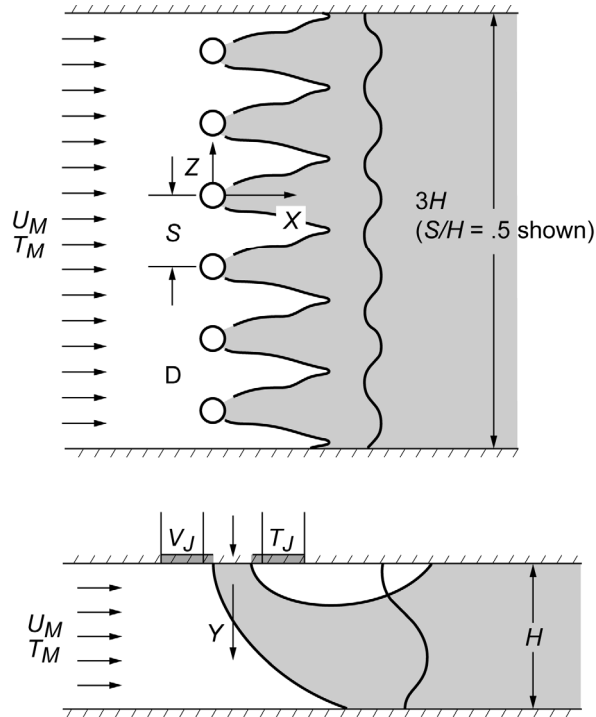
Figure 1.—Schematic for flow field for one side
injection of a row of jets in a confined crossflow.
(Shown for injection from the top duct wall.)
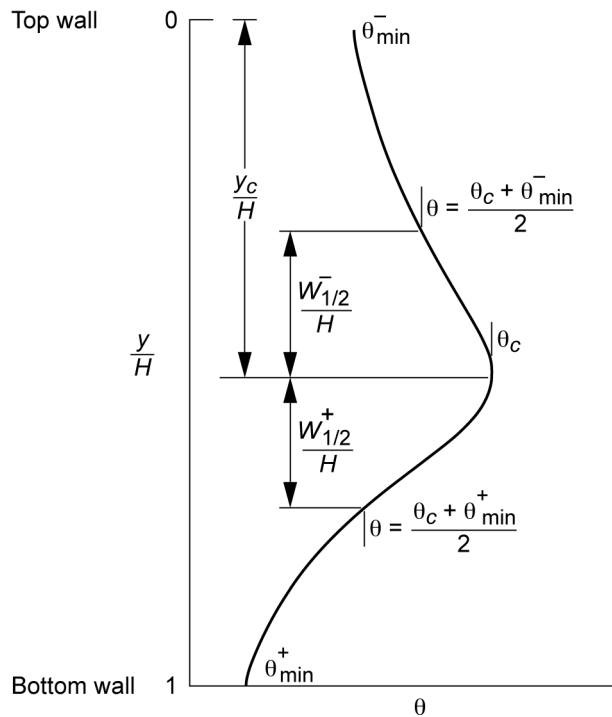
Figure 2.—Schematic of a typical vertical scalar profile
showing scaling parameters in the empirical model.
(Shown for one side injection from the top duct wall.)

Contour Plot

Theta Profile

X

(a) *J* = 6.6

Contour Plot

Theta Profile

(b) *J* = 26,4

Contour Plot

Theta Profile

(c) *J* = 105.6
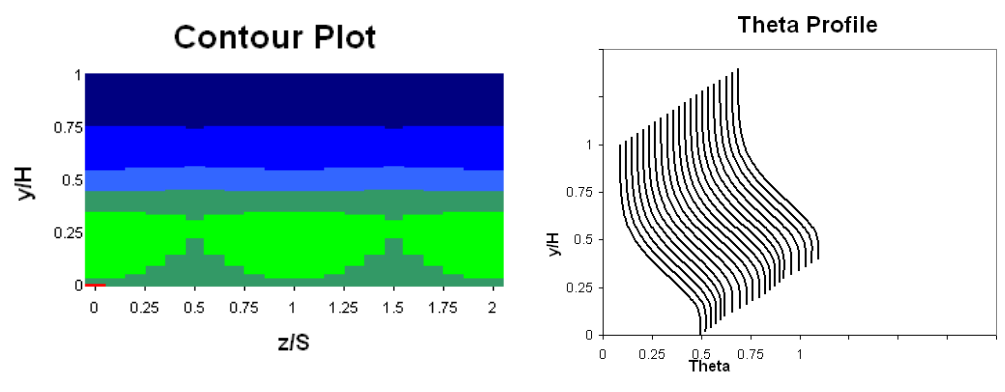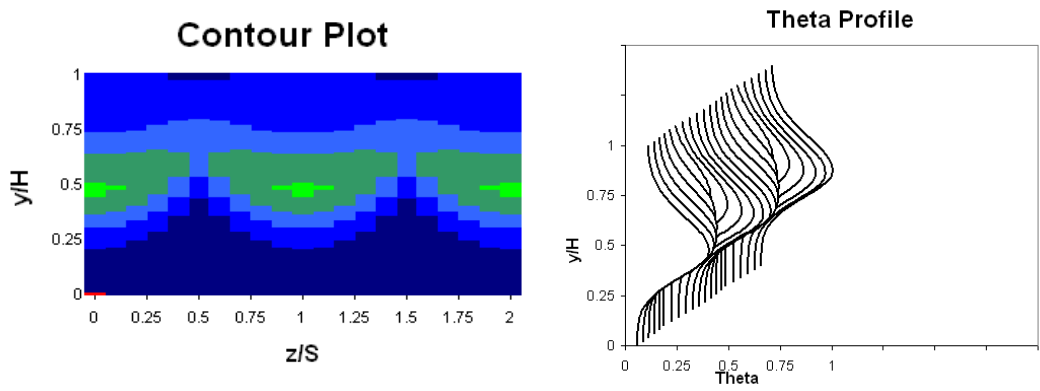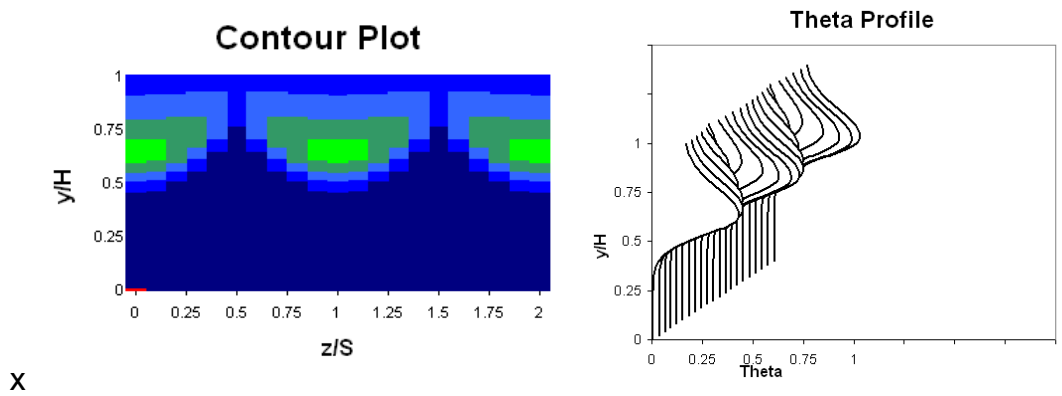
Figure 3.—Variation of scalar distributions with increasing momentum-flux ratio for *S*/*H* = 0.5, *H*/*d* = 5.66, *DR* = 2.2, and C_d = 0.64 at *x*/*H* = 0.5.
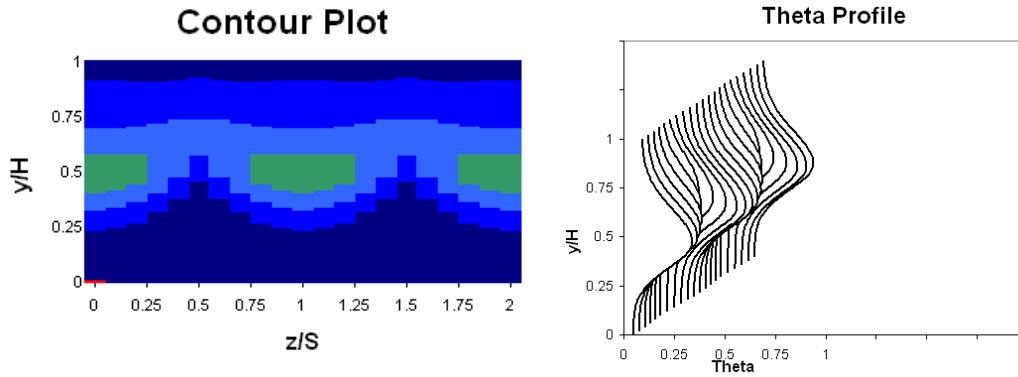
(a) *DR* = 0.5
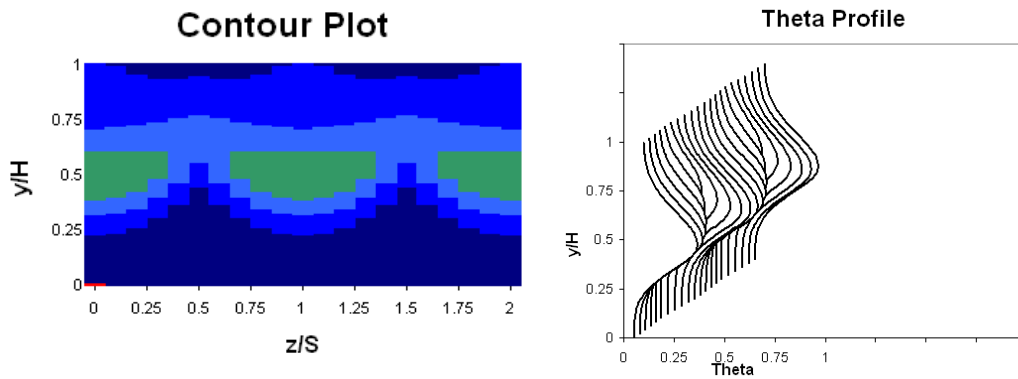
(b) *DR* = 1.0
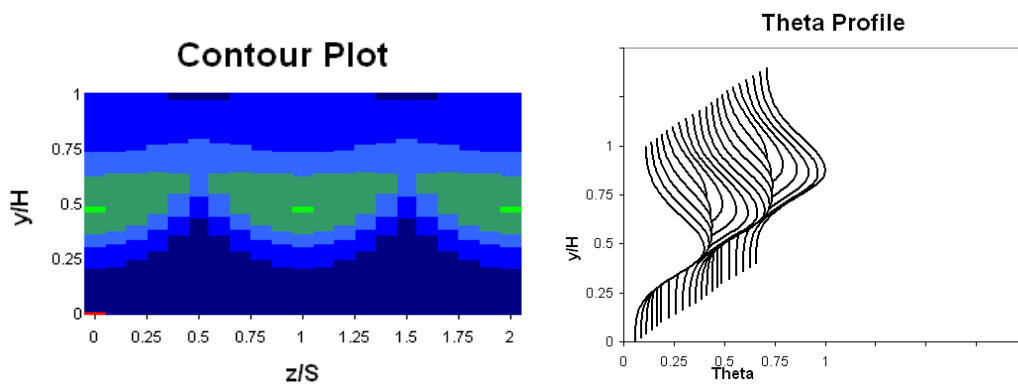
(c) *DR* = 2.0

Figure 4.—Variation of scalar distributions with increasing density ratio for *S*/*H* = 0.5, *H*/*d* = 5.66, *J* = 26.4, and *C*$_d$ = 0.64 at *x*/*H* = 0.5.
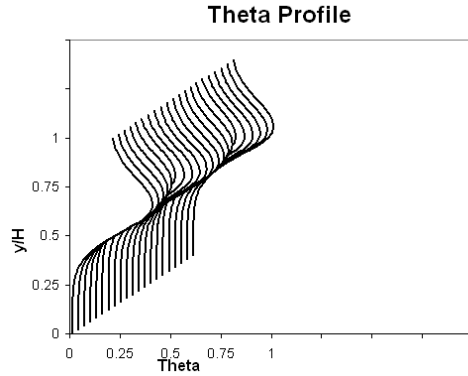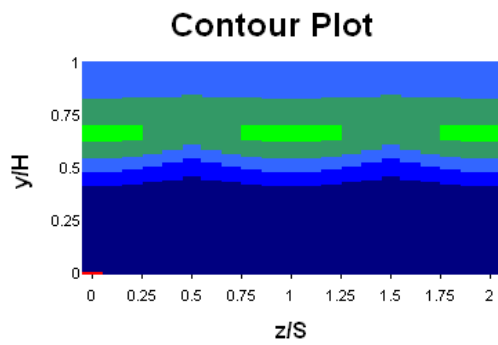
(a) *S/H* = 0.25, (*S/d* = 2)
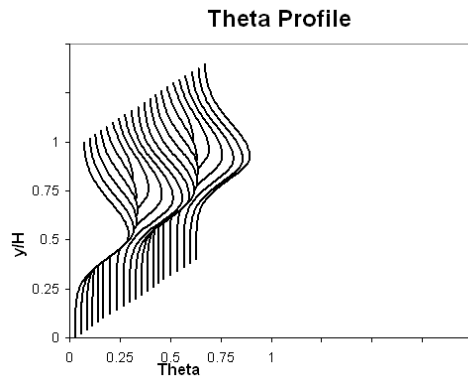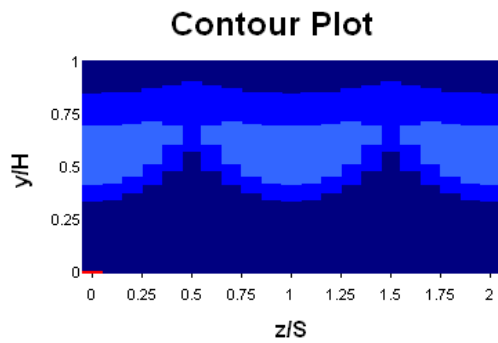
(b) *S/H = 0.5, (S/d = 4)*
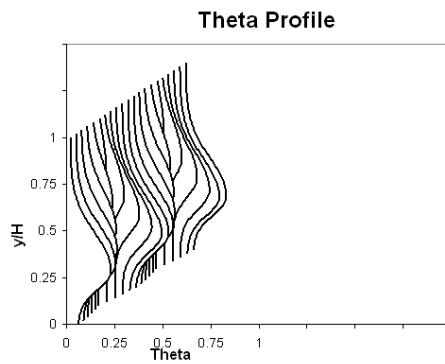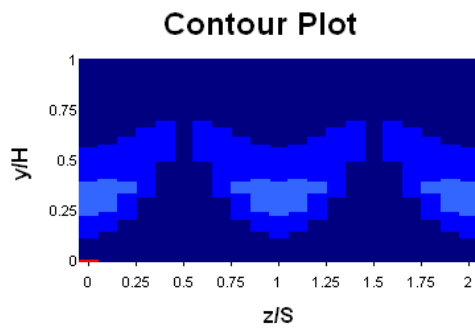
(c) *S/H* = 1.0 (*S/d* = 8)

Figure 5.—Variation of scalar distributions with increasing orifice spacing for H/d = 8, DR = 2.2, J = 26.4, and C_d = 0.64 at x/H = 0.5.
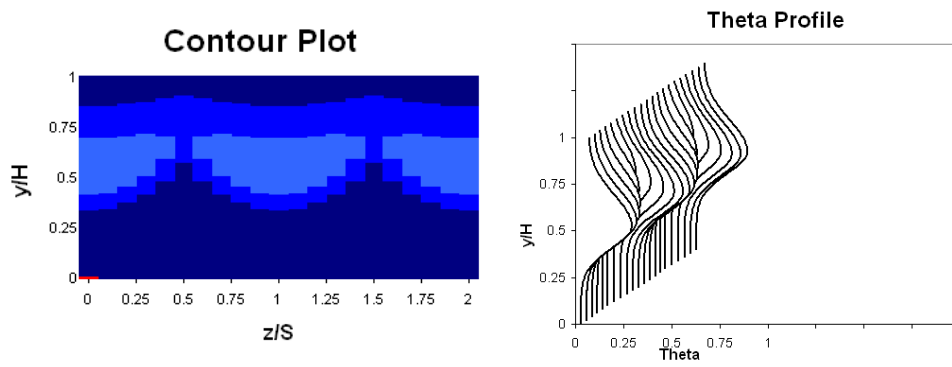
(a) *H/d* = 8 (*S/d* = 4, *x/d* = 4)
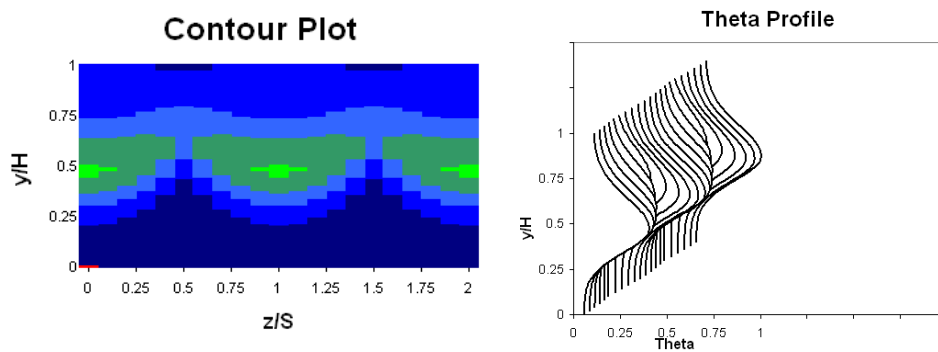
(b) *H/d* = 5.66 (*S/d* = 2.83, *x/d* = 2.83)
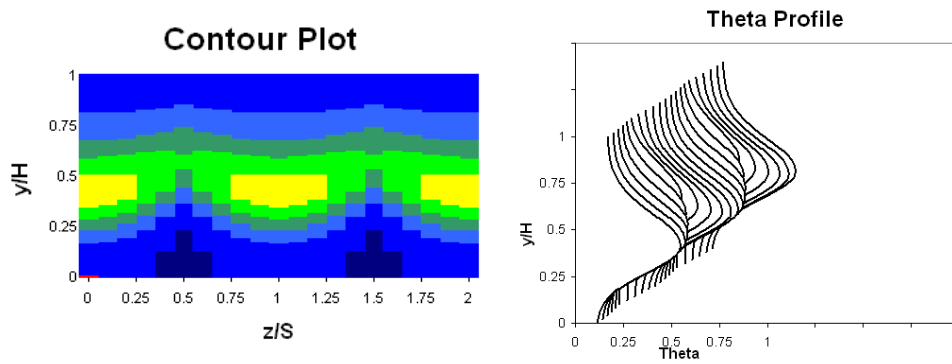
(c) *H/d* = 4 (*S/d* = 2, *x/d* = 2)

Figure 6.—Variation of scalar distributions with increasing orifice diameter (decreasing *H/d*) for *S/H* = 0.5, *DR* = 2.2, *J* = 26.4, and C_d = 0.64 at *x/H* = 0.5.

Contour Plot

y/H

1
0.75
0.5
0.25
0

0   0.25   0.5   0.75   1   1.25   1.5   1.75   2

z/S

Theta Profile

y/H

1
0.75
0.5
0.25

0   0.25   0.5   0.75   1

Theta

(a) *J* = 6.6, *S/H* = 1, *H/d* = 2.83, (*x/d* = 1.42)

Contour Plot

y/H

1
0.75
0.5
0.25
0

0   0.25   0.5   0.75   1   1.25   1.5   1.75   2

z/S

Theta Profile

y/H

1
0.75
0.5
0.25
0

0   0.25   0.5   0.75   1

Theta

(b) *J* = 26.4, *S/H* = 0.5, *H/d* = 5.66, (*x/d* = 2.83)

Contour Plot

y/H

1
0.75
0.5
0.25
0

0   0.25   0.5   0.75   1   1.25   1.5   1.75   2

z/S

Theta Profile

y/H

1
0.75
0.5
0.25
0

0   0.25   0.5   0.75   1

Theta
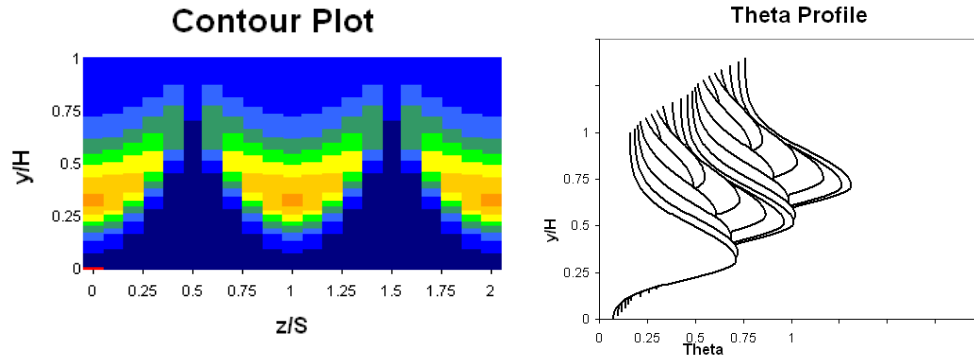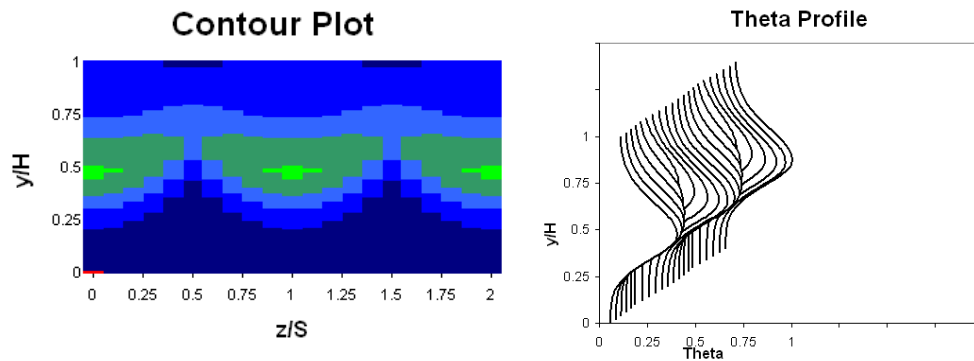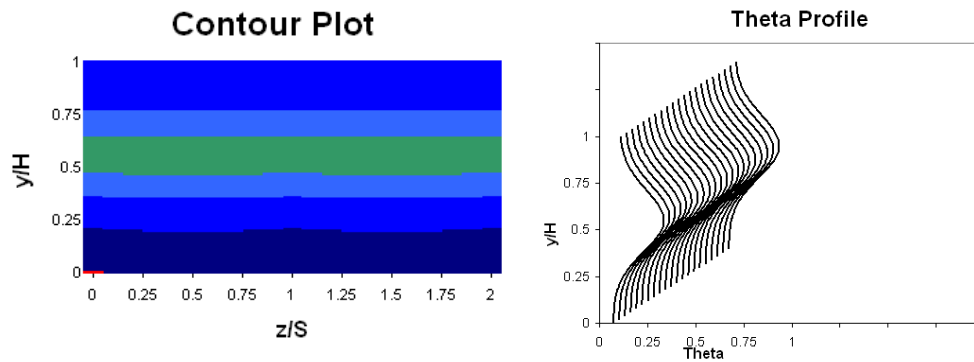
(c) *J* = 105.6, *S/H* = 0.25, *H/d* = 11.32, (*x/d* = 5.66)

Figure 7.—Variation of scalar distributions with coupled momentum-flux ratio (*J*) and orifice spacing (*S/H*) for *DR* = 2.2 and C_d = 0.64 at *x/H* = 0.5. *t x/H* = 0.6.
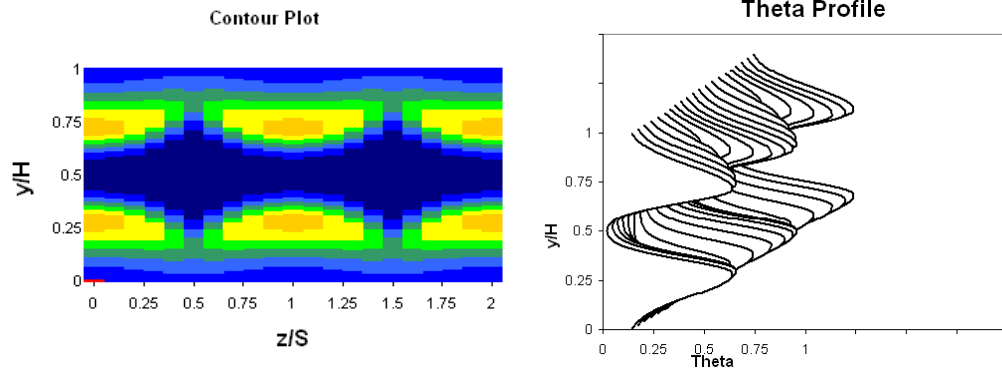
(a) x/H = 0.125 (x/d = 1); U_S = 0.176
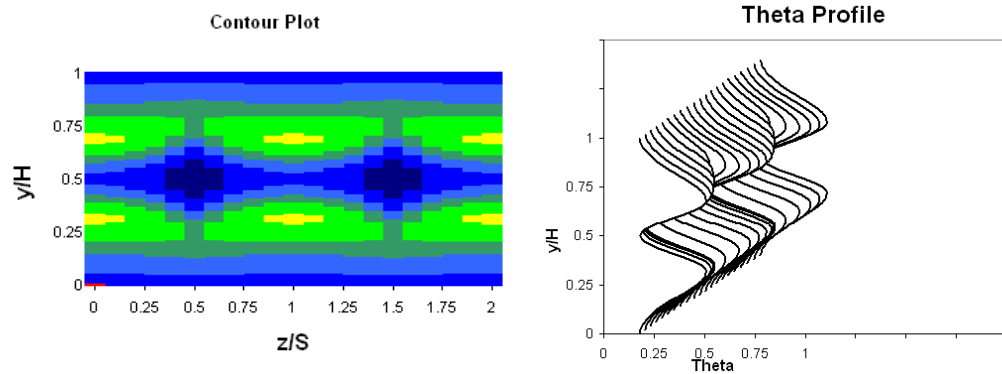
(b) x/H = 0.25 (x/d = 2); U_S = 0.068
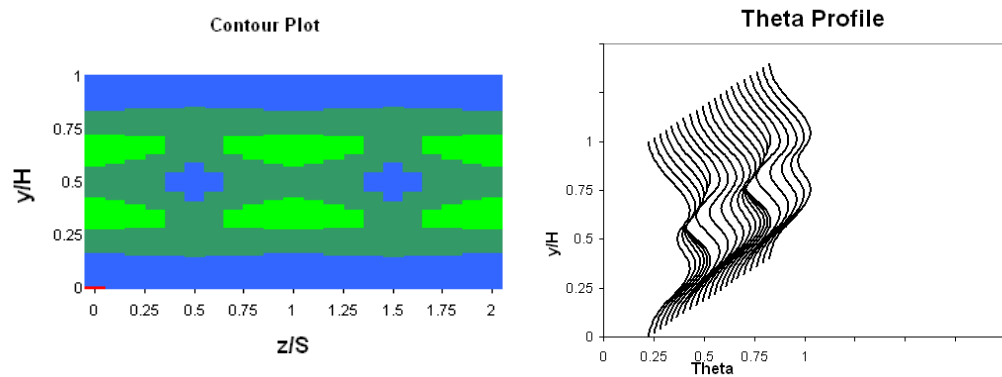
(c) x/H = 0.5 (x/d = 4); U_S = 0.020

Figure 8.—Variation of scalar profile and contour plots for opposed rows of inline jets for S/H = 0.25, H/d = 8 (total A_J/A_M = 0.098), DR = 2.2, J = 26.4, and C_d = 0.64.
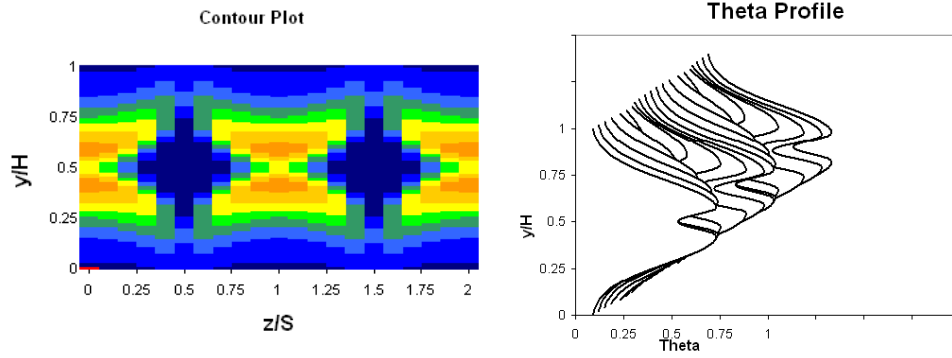
(a) x/H = 0.125 (x/d = 0.71); U_s = 0.185
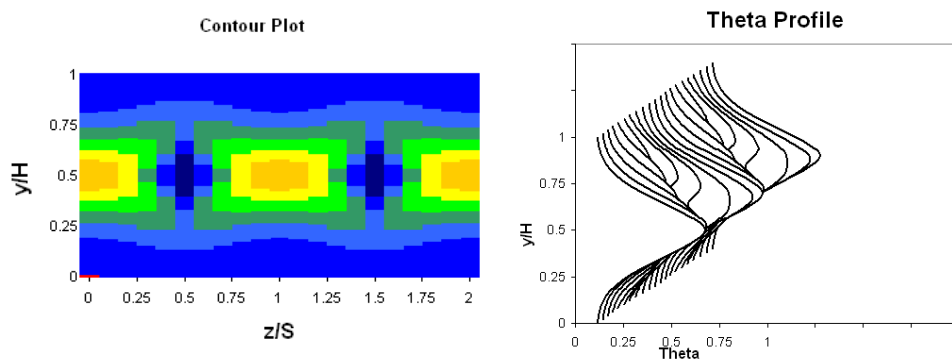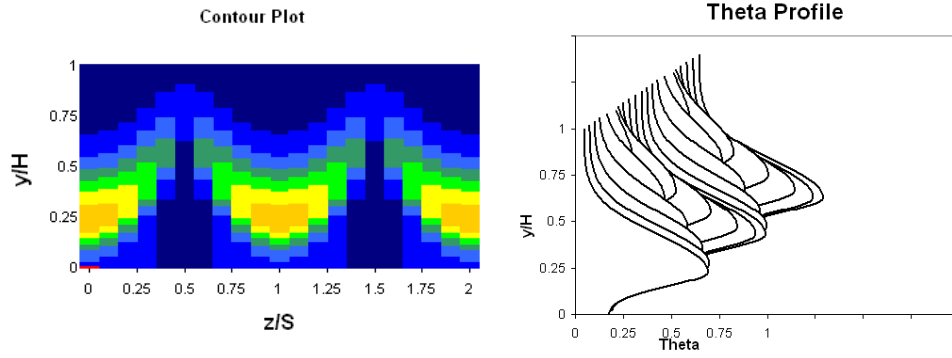

(b) x/H = 0.25 (x/d = 1.41); U_s = 0.113
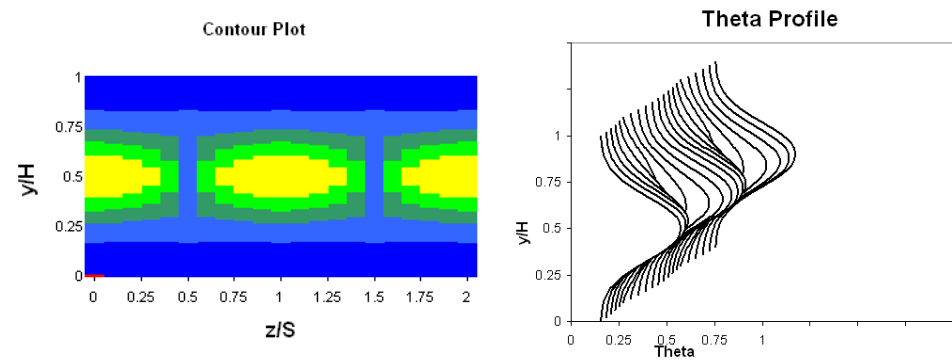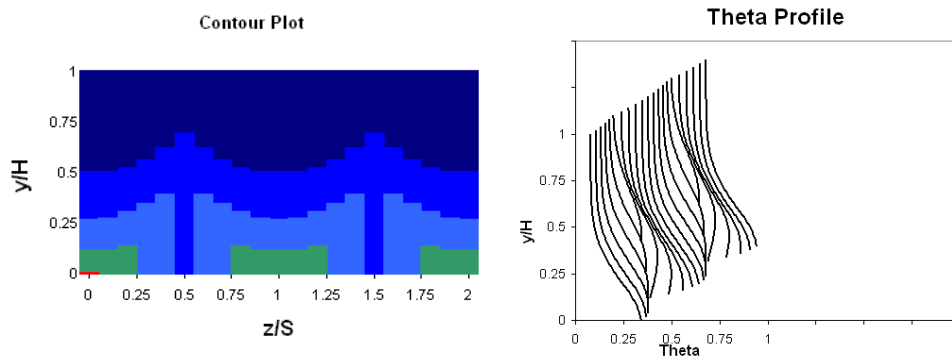

(c) x/H = 0.5 (x/d = 2.83); U_s = 0.084

Figure 9.—Variation of scalar profile and contour plots for opposed rows of inline jets with S/H = 0.5, H/d = 5.66 (total A_J/A_M = 0.098), DR = 2.2, J = 26.4, and C_d = 0.64.
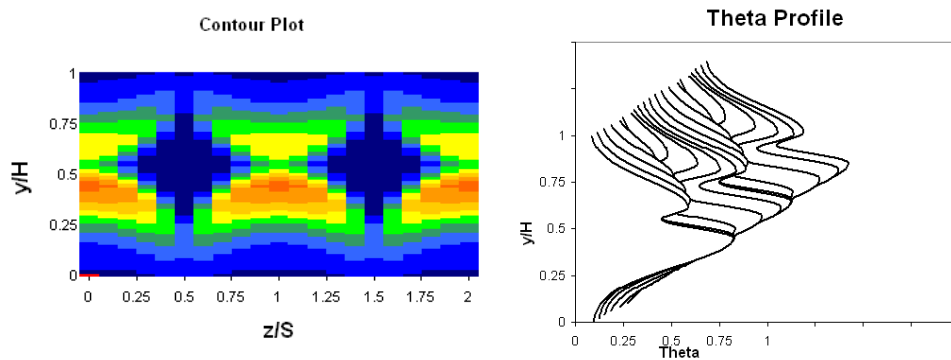
(d)

(a) x/H = 0.125 ($x/d|_{top}$ = 1; $x/d|_{bottom}$ = 0.58). U_S = 0.191
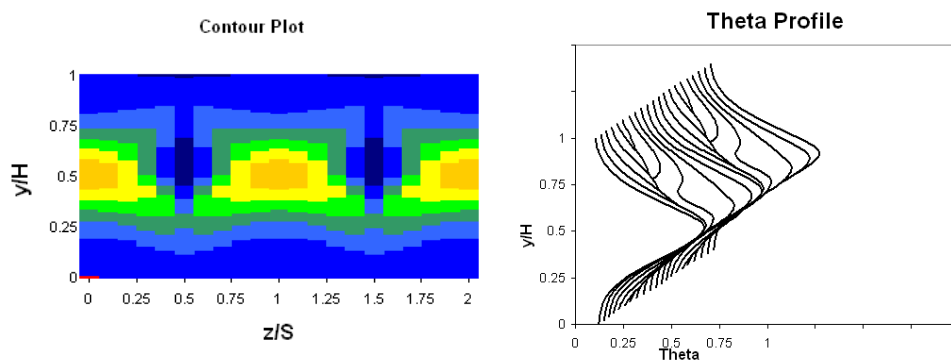
(b) x/H = 0.25 ($x/d|_{top}$ = 2; $x/d|_{bottom}$ = 1.16); U_S = 0.120
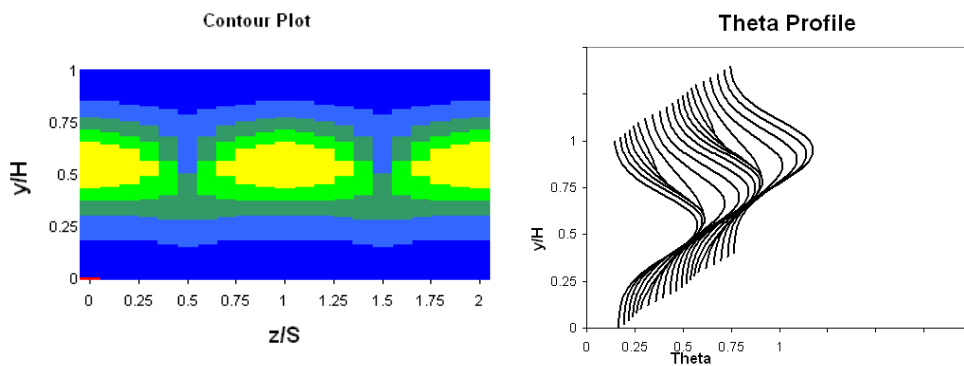
(c) x/H = 0.5 ($x/d|_{top}$ = 4; $x/d|_{bottom}$ = 2.31); U_S = 0.083

Figure 10.—Variation of scalar profile and contour plots for opposed rows of inline jets with S/H = 0.5, H/d = 8 on top, H/d = 4.62 on bottom (total A_J/A_M = 0.098), DR = 2.2, J = 26.4, and C_d = 0.64.
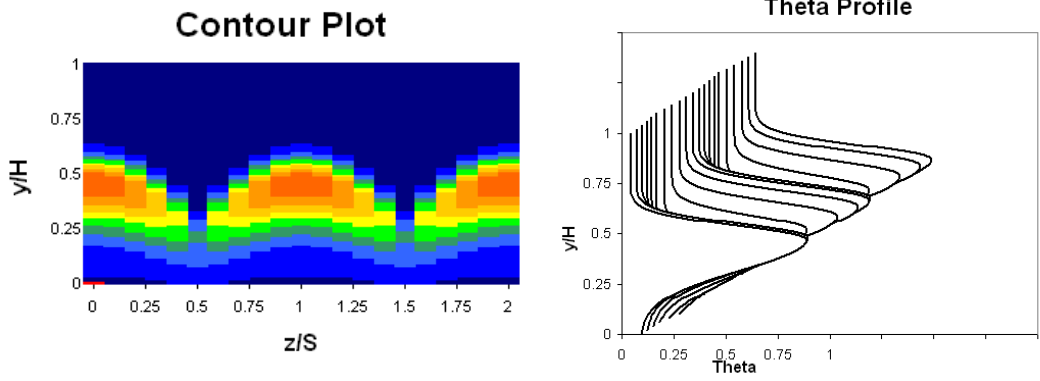
(a) x/H = 0.125 (x/d = 0.5). U_S = 0.318
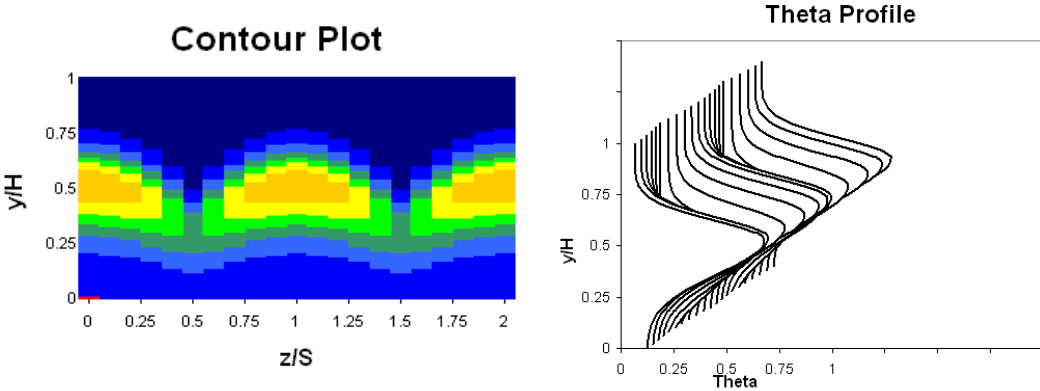
(b) x/H = 0.25 (x/d = 1); U_S = 0.195
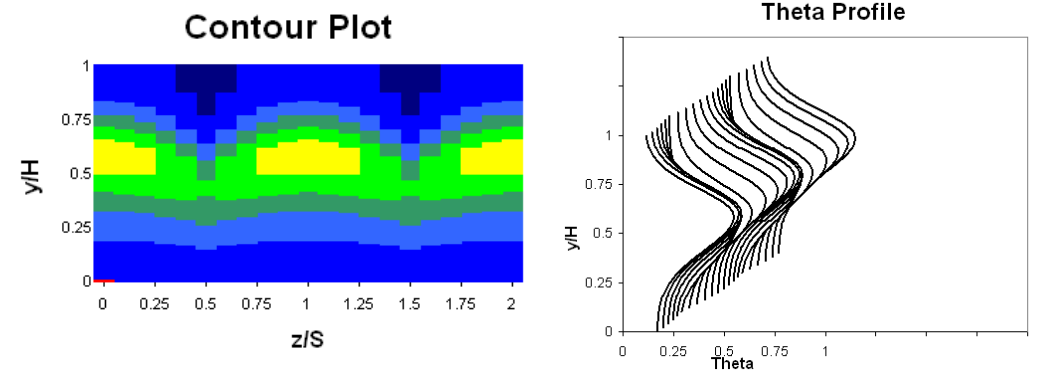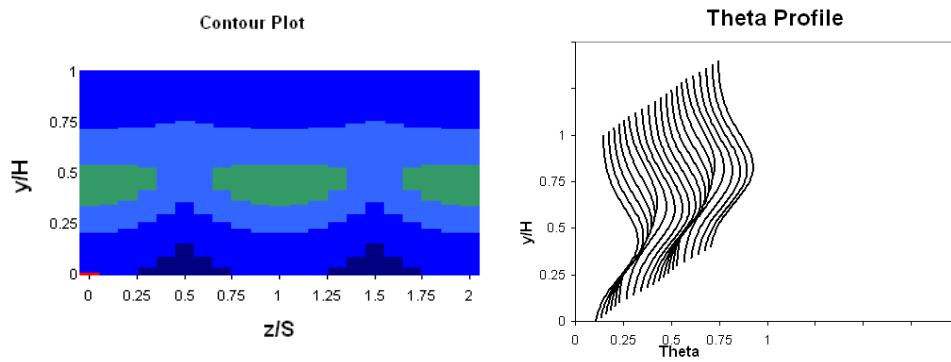

(c) x/H = 0.5 (x/d = 2); U_S = 0.096

Figure 11.—Variation of scalar profile and contour plots for optimum single-side injection with S/H = 0.5, H/d = 4 (A_J/A_M = 0.098), DR = 2.2, J = 26.4, and C_d = 0.64.

Contour Plot

Theta Profile

(a) *x/H* = 0.125 (*x/d* = .5); U_s = 0.406

Contour Plot

Theta Profile

(b) *x/H* = 0.25 (*x/d* = 1); U_s = 0.179

Contour Plot

Theta Profile
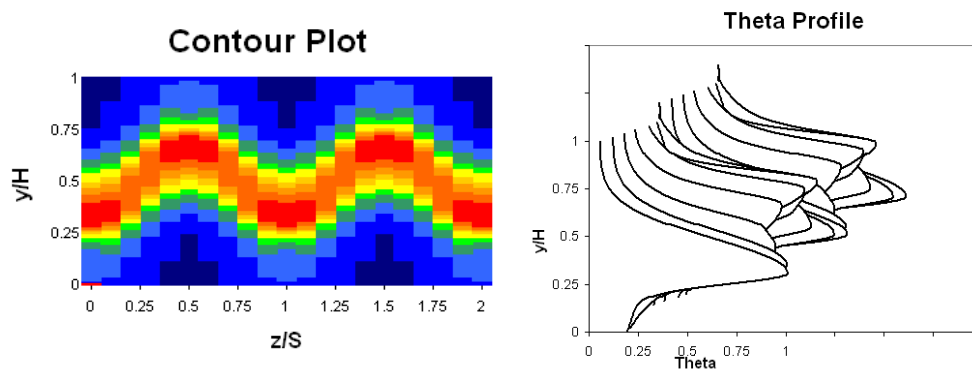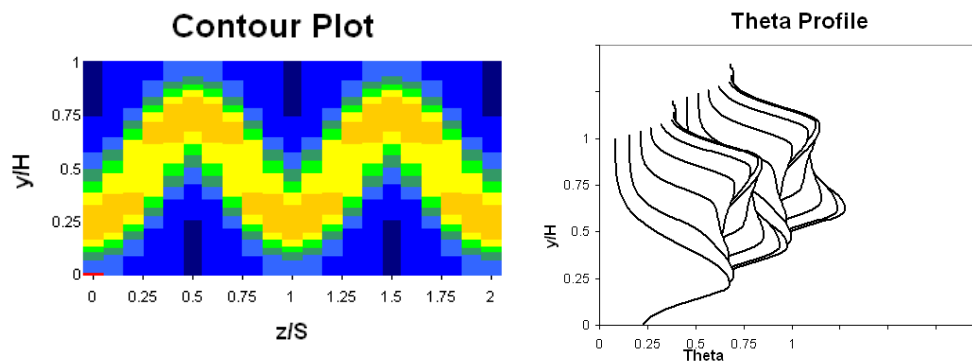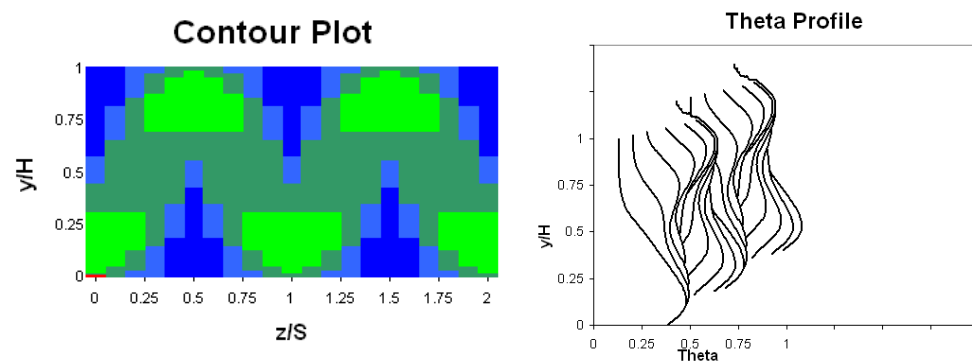
(c) *x/H* = 0.5 (*x/d* = 2); U_s = 0.042

Figure 12.—Variation of scalar profile and contour plots for jets from optimum staggered holes with *S/H* = 1.0, *H/d* = 4 (total A_J/A_M = 0.098), *DR* = 2.2, *J* = 26.4, and C_d = 0.64.
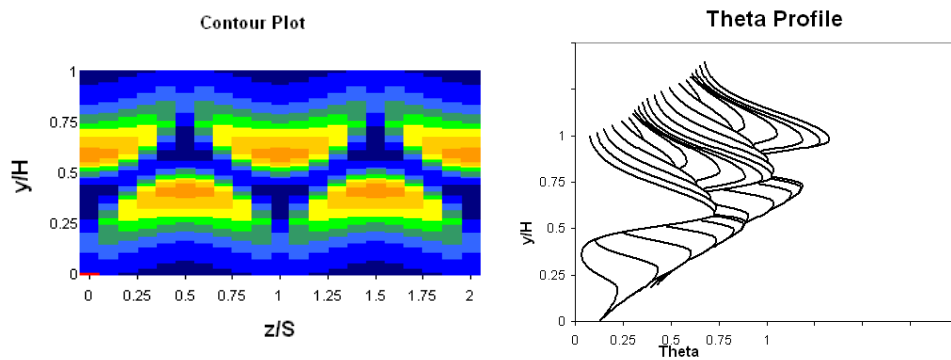
(a) x/H = 0.125 (x/d = .71), U_s = 0.165
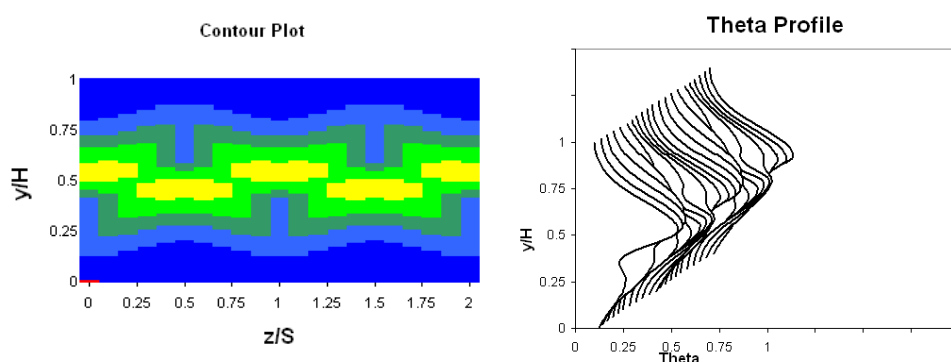
(b) x/H = 0.25 (x/d = 1.42); U_s = 0.091
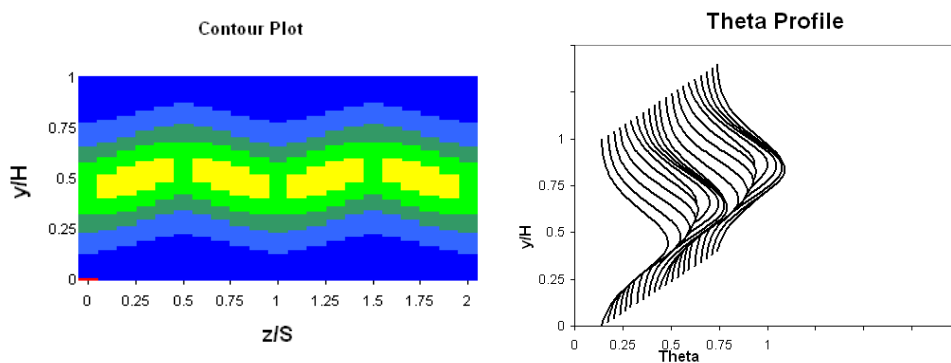
(c) x/H = 0.5 (x/d = 2.83); U_s = 0.083

Figure 13.—Variation of scalar profile and contour plots for opposing rows of staggered jets with S/H = 0.5, H/d = 5.66 (total A_J/A_M = 0.098), DR = 2.2, J = 26.4, and C_d = 0.64.
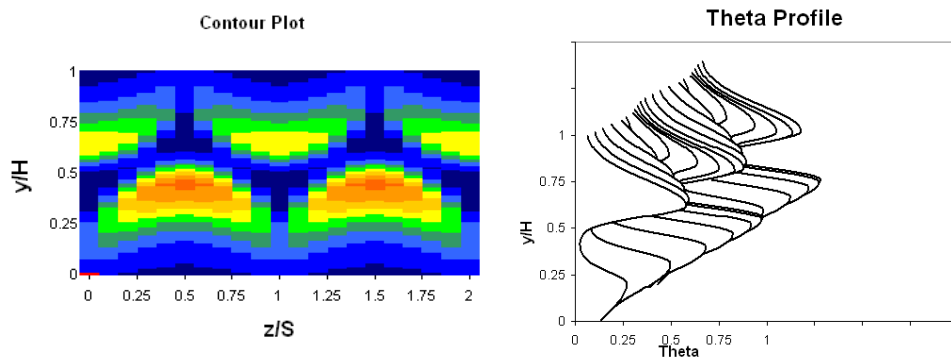
(a) x/H = 0.125 ($x/d|_{top}$ = 1; $x/d|_{bottom}$ = 0.58); U_S = 0.176
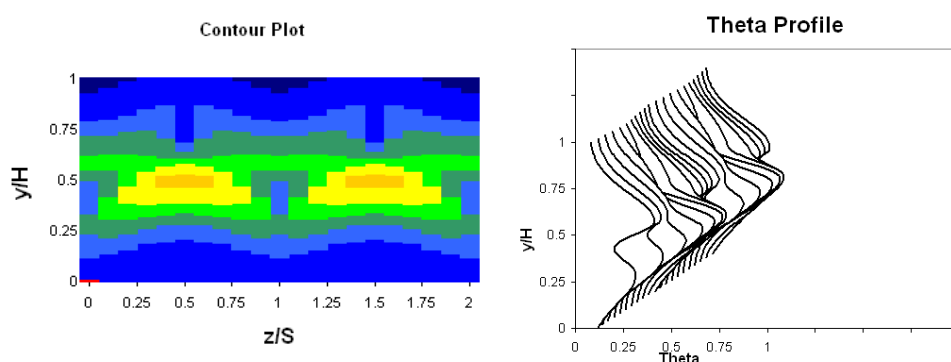
(b) x/H = 0.25 ($x/d|_{top}$ = 2; $x/d|_{bottom}$ = 1.16); U_S = 0.097
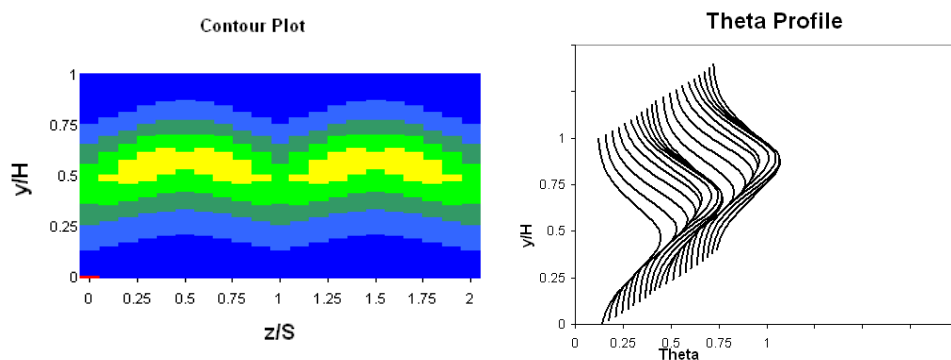
(c) x/H = 0.5 ($x/d|_{top}$ = 4; $x/d|_{bottom}$ = 2.31); U_S = 0.081

Figure 14.—Variation of scalar profile and contour plots for opposing rows of staggered jets with H/d = 8 on top, H/d = 4.62 on bottom (total A_J/A_M = 0.098), for S/H = 0.5, DR = 2.2, J = 26.4, and C_d = 0.64.
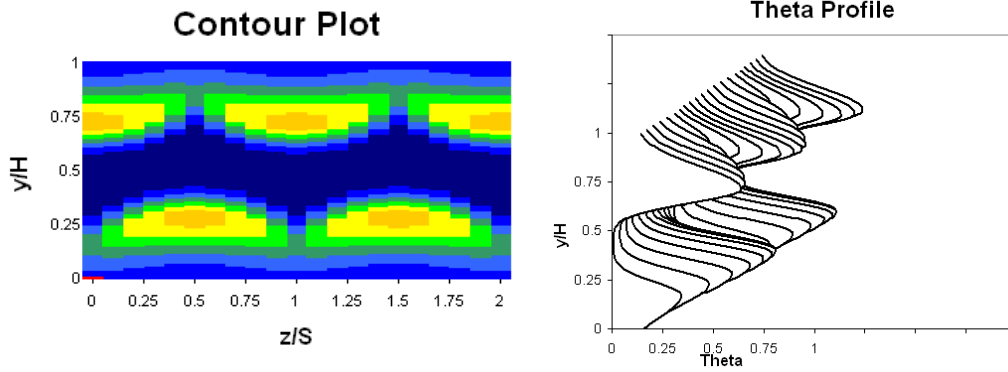
(a) x/H = 0.125 (x/d = 1); U_s = 0.175
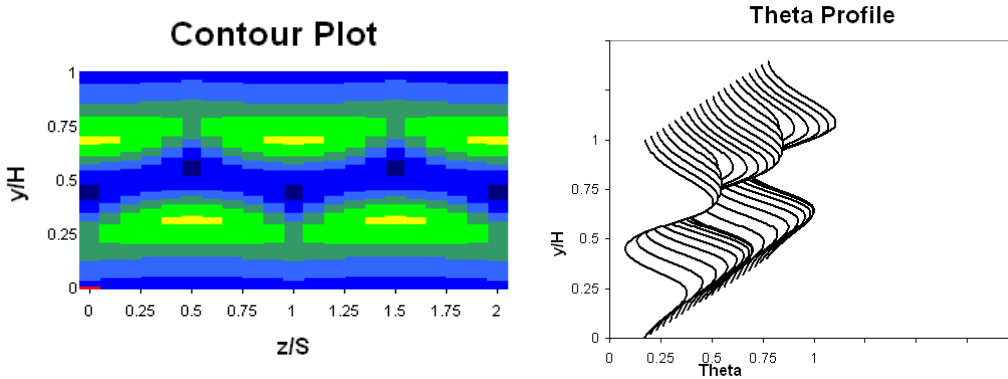
(b) x/H = 0.25 (x/d = 2); U_s = 0.065
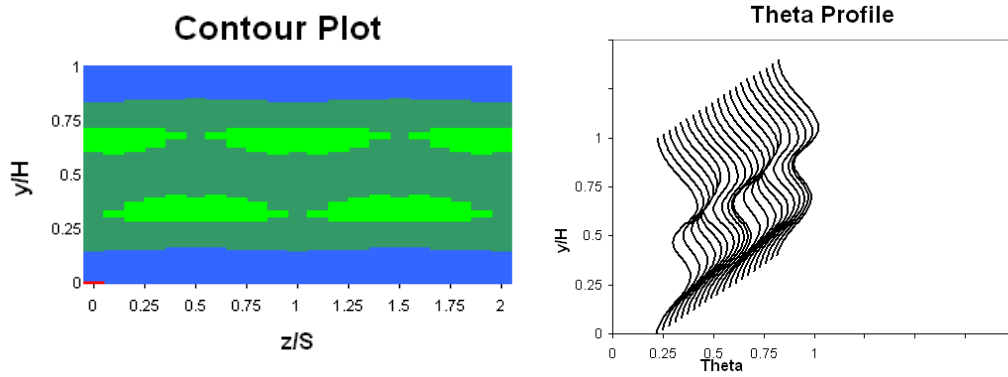
(c) x/H = 0.5 (x/d = 4); U_s = 0.018

Figure15.—Variation of scalar profile and contour plots for opposed rows of staggered jets for S/H = 0.25, H/d = 8 (total A_J/A_M = 0.098), DR = 2.2, J = 26.4, and C_d = 0.64.

(a) x/H = 0.25 (x/d = 1); U_S = 0.199
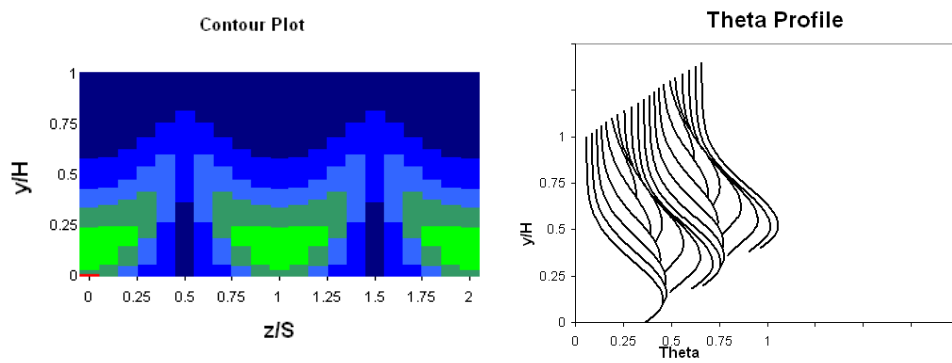
(b) x/H = 0.5 (x/d = 2), U_S = 0.099

(c) x/H = 1.0 (x/d = 4); U_S = 0.056

Figure 16.—Variation of scalar profile and contour plots for one side injection with S/H = 1.0, H/d = 4 (A_J/A_M = 0.049), DR = 2.2, J = 26.4, and C_d = 0.64.
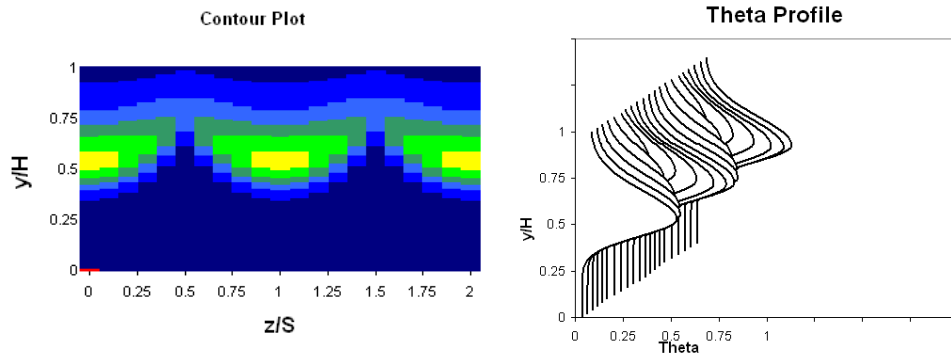
(a) x/H = 0.25 (x/d = 1.42); U_s = 0.149
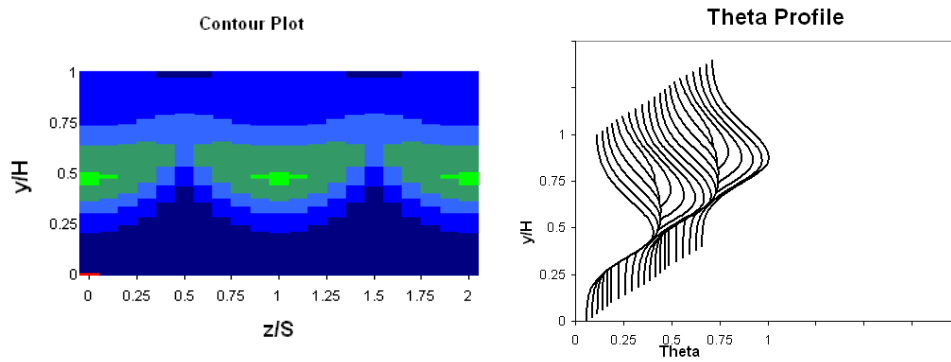
(b) x/H = 0.5 (x/d = 2.83). U_s = 0.078

(c) x/H = 1.0 (x/d = 5.66); U_s = 0.032

Figure 17.—Variation of scalar profile and contour plots for one side injection with S/H = 0.5, H/d = 5.66 (A_J/A_M = 0.049), DR = 2.2, J = 26.4, and C_d = 0.64.
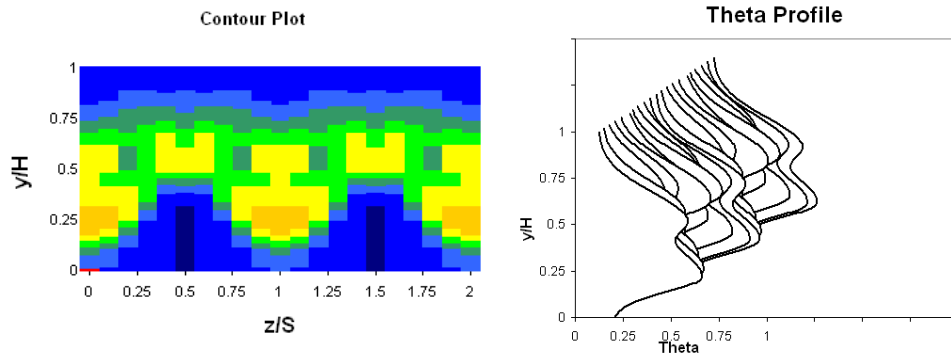
(a) x/H = 0.25; U_s = 0.177
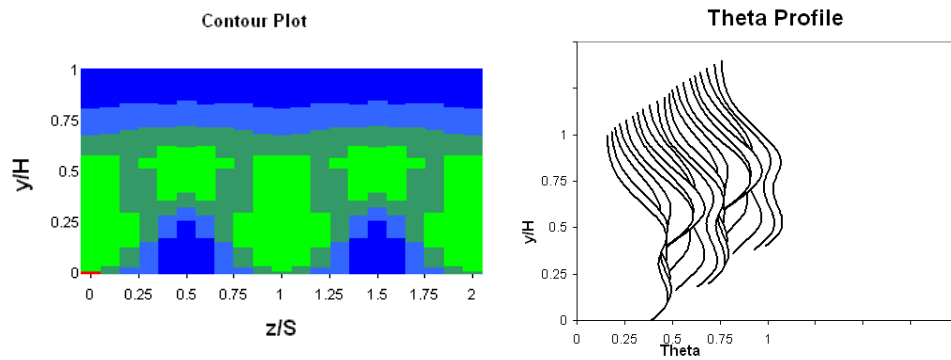
(b) x/H = 0.5; U_s = 0.099
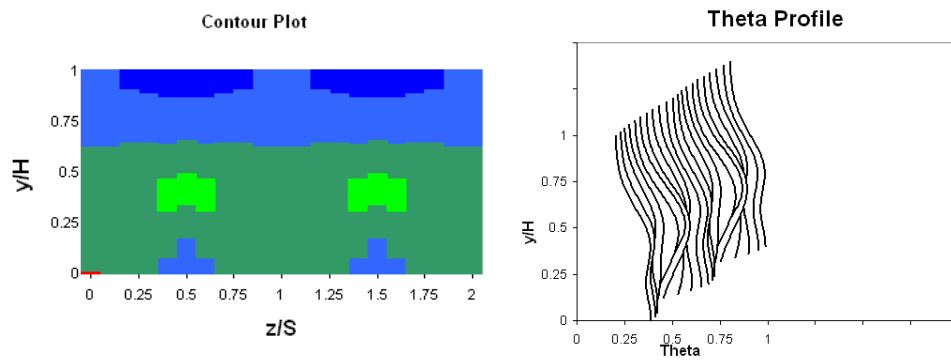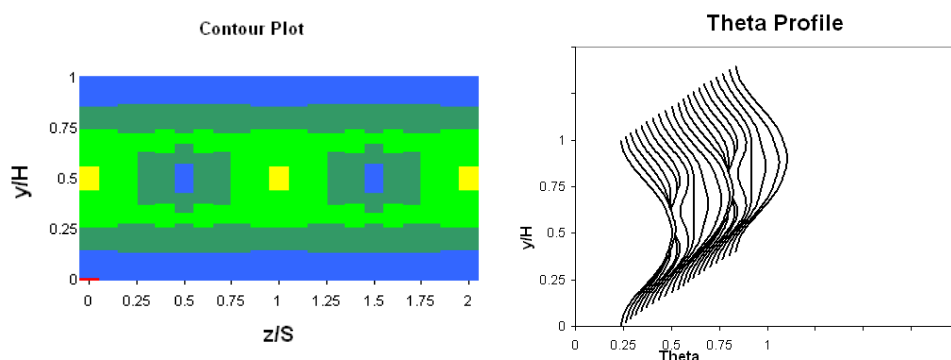

(c) x/H = 1.0; U_s = 0.028

Figure 18.—Variation of scalar profile and contour plots for one side injection from alternating size holes for S/H = 1.0, H/d = 4 in row 1 and S/H = 0.5, H/d = 5.66 in row 2 with S_x/H = 0 (total A_J/A_M = 0.098), DR = 2.2, J = 26.4, and C_d = 0.64.
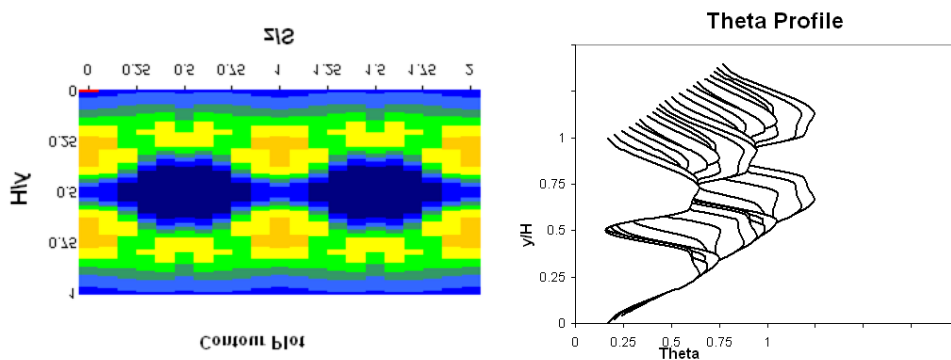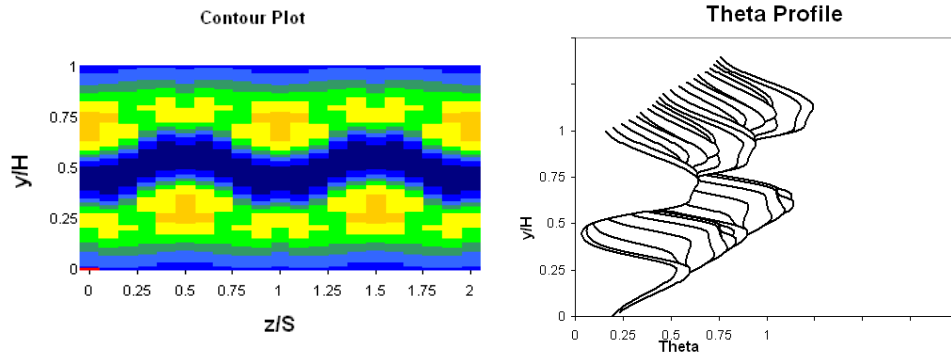
(a) x/H = 0.125; U_s = 0.153
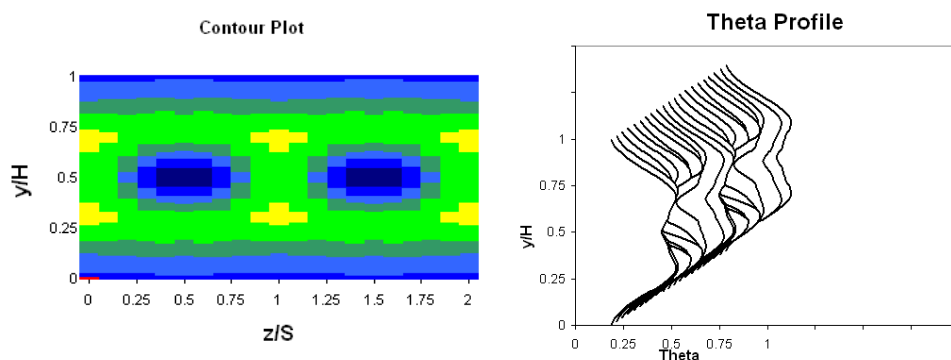
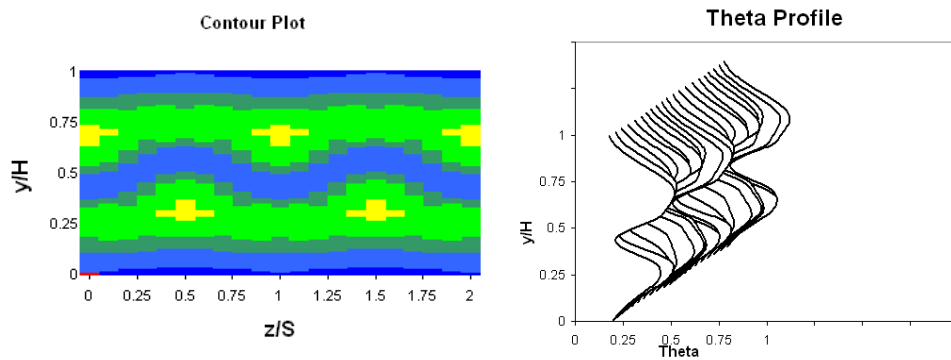(b) x/H = 0.25; U_s = 0.061

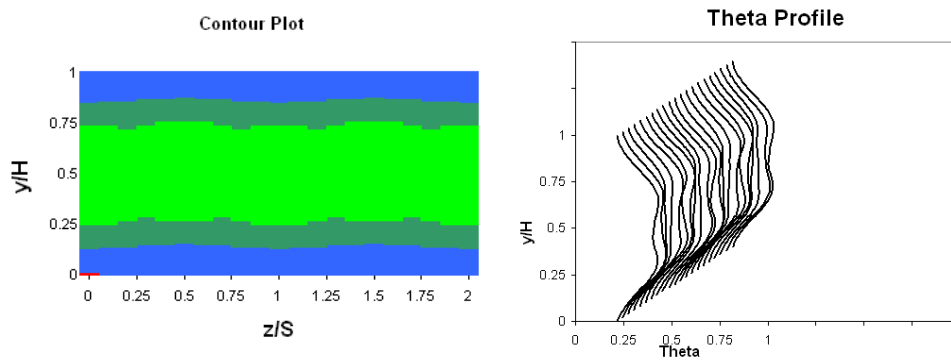
(c) x/H = 0.5; U_s = 0.034

Figure 19.—Variation of scalar profile and contour plots for opposed rows of alternating hole sizes with similar holes opposite each other for S/H = 0.5, H/d = 8 and S/H = 0.25, H/d = 11.31 on each side with S_x/H = 0 (total A_J/A_M = 0.098), DR = 2.2, J = 26.4, and C_d = 0.64.

(a) x/H = 0.125; U_s = 0.149

(b) x/H = 0.25; U_s = 0.047

(c) x/H = 0.5; U_s = 0.029

Figure 20.—Variation of scalar profile and contour plots for opposed rows of alternating hole sizes with large and small holes opposite each other for S/H = 0.5, H/d = 8 and S/H = 0.25, H/d = 11.31 on each side with S_x/H = 0 (total A_J/A_M = 0.098), DR = 2.2, J = 26.4, and C_d = 0.64.

1. REPORT DATE (DD-MM-YYYY) 01-07-2010	2. REPORT TYPE Technical Memorandum	3. DATES COVERED (From - To)

4. TITLE AND SUBTITLE
Spreadsheet Calculations for Jets in Crossflow: Opposed Rows of Inline and Staggered Holes and Single and Opposed Rows With Alternating Hole Sizes

5a. CONTRACT NUMBER

5b. GRANT NUMBER

5c. PROGRAM ELEMENT NUMBER

6. AUTHOR(S)
Holdeman, James, D.; Clisset, James, R.; Moder, Jeffrey, P.

5d. PROJECT NUMBER

5e. TASK NUMBER

5f. WORK UNIT NUMBER
WBS 561581.02.08.03.16.03

7. PERFORMING ORGANIZATION NAME(S) AND ADDRESS(ES)
National Aeronautics and Space Administration
John H. Glenn Research Center at Lewis Field
Cleveland, Ohio 44135-3191

8. PERFORMING ORGANIZATION REPORT NUMBER
E-17185

9. SPONSORING/MONITORING AGENCY NAME(S) AND ADDRESS(ES)
National Aeronautics and Space Administration
Washington, DC 20546-0001

10. SPONSORING/MONITOR'S ACRONYM(S)
NASA

11. SPONSORING/MONITORING REPORT NUMBER
NASA/TM-2010-216100

12. DISTRIBUTION/AVAILABILITY STATEMENT
Unclassified-Unlimited
Subject Category: 07
Available electronically at http://gltrs.grc.nasa.gov
This publication is available from the NASA Center for AeroSpace Information, 443-757-5802

13. SUPPLEMENTARY NOTES
Jim Holdeman, retired. A supplemental Microsoft Excel (Microsoft Corporation) spreadsheet TM-2010-216100-SUPPL1.xls can be viewed on the Web at http://gltrs.grc.nasa.gov.

14. ABSTRACT
The primary purpose of this jet-in-crossflow study was to calculate expected results for two configurations for which limited or no experimental results have been published: (1) cases of opposed rows of closely-spaced jets from inline and staggered round holes and (2) rows of jets from alternating large and small round holes. Simulations of these configurations were performed using an Excel (Microsoft Corporation) spreadsheet implementation of a NASA-developed empirical model which had been shown in previous publications to give excellent representations of mean experimental scalar results suggesting that the NASA empirical model for the scalar field could confidently be used to investigate these configurations. The supplemental Excel spreadsheet is posted with the current report on the NASA Glenn Technical Reports Server (http://gltrs.grc.nasa.gov) and can be accessed from the Supplementary Notes section as TM-2010-216100-SUPPL1.xls. Calculations for cases of opposed rows of jets with the orifices on one side shifted show that staggering can improve the mixing, particularly for cases where jets would overpenetrate slightly if the orifices were in an aligned configuration. The jets from the larger holes dominate the mixture fraction for configurations with a row of large holes opposite a row of smaller ones although the jet penetration was about the same. For single and opposed rows with mixed hole sizes, jets from the larger holes penetrated farther. For all cases investigated, the dimensionless variance of the mixture fraction decreased significantly with increasing downstream distance. However, at a given downstream distance, the variation between cases was small.

15. SUBJECT TERMS
Jets in crossflow; Gas turbine combustors

16. SECURITY CLASSIFICATION OF:			17. LIMITATION OF ABSTRACT	18. NUMBER OF PAGES	19a. NAME OF RESPONSIBLE PERSON STI Help Desk (email:help@sti.nasa.gov)
a. REPORT U	b. ABSTRACT U	c. THIS PAGE U	UU	39	19b. TELEPHONE NUMBER (include area code) 443-757-5802